Eur. Phys. J. C (2024) 84:132
https://doi.org/10.1140/epjc/s10052-024-12493-3

THE EUROPEAN PHYSICAL JOURNAL C

Regular Article - Theoretical Physics

Fatjet signatures of heavy neutrinos and heavy leptons in a left-right model with universal seesaw at the HL-LHC

Atri Dey[a], **Rafiqul Rahaman**[b], **Santosh Kumar Rai**[c],

Regional Centre for Accelerator-based Particle Physics, Harish-Chandra Research Institute, A CI of Homi Bhabha National Institute, Chhatnag Road, Jhunsi, Prayagraj 211019, India

Received: 28 March 2023 / Accepted: 29 January 2024 / Published online: 7 February 2024

Abstract We perform a collider search for fatjet signals originating from boosted heavy neutral and charged leptons with masses between a few hundred GeV to a TeV. These heavy leptons originate from the decay of heavy gauge bosons with masses above 4 TeV in a left-right symmetric extension of the Standard Model (SM), which considers a universal seesaw mechanism for the generation of all the SM fermion masses. The fatjet signals arise naturally in this model due to the presence of heavy seesaw partners of the SM fermions which decay to SM gauge bosons carrying large boosts. We employ substructure based variables lepton subjet fraction (LSF) and lepton mass drop (LMD) together with kinematic variables of fatjets to look for fatjet signals associated with non-isolated leptons. These variables help in reducing the SM backgrounds while retaining enough statistics for signal events, which leads to a robust discovery potential at the high-luminosity Large Hadron Collider (HL-LHC).

1 Introduction

Non zero neutrino mass observed in experiments [1–5] is one of the key hints to look for physics beyond the Standard Model (SM). Some other aspects unexplained in the SM are dark matter, hierarchy of masses in the three known fermion generations, gauge hierarchy problem, Baryogenesis, CP-violation, etc. Left-right symmetric extension of the SM (LRSM) [6–9] is one of the well motivated models of new physics, which offers an explanation for some of the experimental as well as theoretical limitations of the SM mentioned above. Left-right symmetric models resolve the issue of maximal parity violation in the weak sector and naturally accommodate right-handed neutrinos in the framework which leads to the popular seesaw mechanism for neutrino mass generation [10–13]. The seesaw framework gives rise to Majorana masses to the neutrinos and the heavy neutrinos have lepton-number violating interactions. These heavy states can decay via their CP-violating Yukawa interactions to generate a lepton asymmetry. This lepton asymmetry is then partially converted to a baryon asymmetry through the SM sphaleron processes that can explain the matter–antimatter asymmetry [14–17]. The LRSM models also account for CP-violation and resolve the strong CP problem [18–23].

The minimal left-right models include scalar triplets and a scalar bi-doublet along with right-handed SM fermions arranged in the $SU(2)_R$ as doublets [24]. This leads to the SM neutrinos getting their eventual mass via the seesaw mechanism, while the rest of the SM fermions get mass through their Yukawa interactions with the bidoublet scalar in the usual manner. We adopt an LRSM framework that suggests that all SM fermions, including the neutrinos, get their mass from a seesaw mechanism similar to that of the neutrino [25]. This can be achieved by modifying the scalar sector of LRSM with four $SU(2)$ doublet scalars, one each for the lepton and quark doublets in the left sector as well as in the right sector [25,26]. A big advantage of generating the fermion masses in this manner is to prevent a highly hierarchical Yukawa structure, like in the SM. The fermion sector, however, also gets modified and heavy singlet charged fermions along with heavy singlet Majorana neutrinos need to be included to achieve a universal seesaw mechanism for the generation of all the fermion masses. In such models, even the strong CP problem is resolved without an axion if a discrete parity symmetry is imposed [27].

This framework offers rich and interesting phenomenology whose signals can be observed at current and future colliders. An interesting signal for the model will be the obser-

[a] e-mail: atridey@hri.res.in
[b] e-mail: rafiqulrahaman@hri.res.in (corresponding author)
[c] e-mail: skrai@hri.res.in

vation of fatjet signatures of heavy neutrinos (ν_i) and exotic heavy charged leptons (E_i) with masses around a few hundred GeV to TeV. This signal originates from the decay of the heavy right-handed charged gauge boson (W_R) with mass above a few TeV. We note that fatjet signatures of heavy neutrinos have been studied in the literature for LRSM models with minimal scalar sector that generate seesaw masses for neutrinos [28–30] at the Large Hadron Collider (LHC). However, in the universal seesaw model, the presence of heavy charged fermions along with the heavy Majorana neutrinos[1] lead to an even more interesting picture of final states with multiple fatjets and different lepton charge multiplicities. The signal originates from the production of the W_R via pp collision, which then decays to a heavy neutrino and a heavy charged lepton. The heavy lepton further decays to a heavy neutrino and a pair of jets via an off-shell W_R. Each of the heavy neutrinos (dominantly right-handed) further decay to a lepton and a pair of jets through off-shell W_R. The heavy neutrinos being much lighter than the W_R are produced with a substantial boost, and their decay products (pair of jets including a charged lepton) form boosted fatjets. The emerging signal becomes a topology of three fatjets where two of them include a lepton and one is characterized by two sub-jets. This three-fatjet signal results from the following sub-process in the model,

$$pp \to W_R \to E_i \nu_j,\ E_i \to \nu_k W_R^\star,\\ \nu_k \to jj(W_R^\star) l_i^\pm,\ W_R^\star \to jj. \tag{1}$$

This LRSM framework also offers two-fatjet signals including a lepton, originating from the decay of the heavy right-handed neutral gauge boson (Z_R):

$$pp \to Z_R \to \nu_i \nu_j,\ \nu_i \to l_k^\pm jj. \tag{2}$$

Interestingly, a possibility of a more exotic signal including four fatjets also exists because of the production of the heavy charged leptons E_i produced via

$$pp \to Z_R \to E_i E_j. \tag{3}$$

A complete account of the possible signals is given in Sect. 4. We note that the presence of leptons in the fatjet can be a crucial identification since the leptons and jets produced from the decay of the boosted heavy neutrinos are mostly non-isolated, following the standard isolation criteria used by the CMS and ATLAS [31,32] Collaborations. We, therefore, use substructure-based variables employed by the experimental collaborations called lepton sub-jet fraction (LSF) and lepton mass drop (LMD) to distinguish our fatjet signal from the non-reducible quantum chromodynamics (QCD) background [33]. These variables (LSF, LMD) will be defined later in Sect. 4.

The rest of the paper is organized as follows. We give a brief description of the LRSM model with a universal seesaw mechanism in Sect. 2. In Sect. 3, we discuss the constraints on the model parameters and phenomenologically allowed benchmark points for our analysis. In Sect. 4, we present our collider analysis and results using the variables LSF and LMD. We conclude with our findings in Sect. 5.

2 The Model

A brief description of the model [25] is given below. The left-right symmetric model is based on the gauge group $SU(3)_C \times SU(2)_L \times SU(2)_R \times U(1)_{B-L}$ along with an extra Z_2 symmetry to incorporate a lepton-specific scenario. The charge of a particle is defined as

$$\mathcal{Q} = I_{3L} + I_{3R} + \frac{B-L}{2}. \tag{4}$$

The particle spectrum of the model along with their quantum number and Z_2 charges are shown in Table 1. The matter structure consists of three families of $SU(2)_L$ and $SU(2)_R$ quark and lepton doublets,

$$Q_L = \begin{pmatrix} u \\ d \end{pmatrix}_L \sim \left(3, 2, 1, \frac{1}{3}\right),\ Q_R = \begin{pmatrix} u \\ d \end{pmatrix}_R \sim \left(3, 1, 2, \frac{1}{3}\right),\\ l_L = \begin{pmatrix} \nu \\ e \end{pmatrix}_L \sim (1, 2, 1, -1),\ l_R = \begin{pmatrix} \nu \\ e \end{pmatrix}_R \sim (1, 1, 2, -1), \tag{5}$$

where the numbers in the parentheses denote the quantum numbers under $SU(3)_C \times SU(2)_L \times SU(2)_R \times U(1)_{B-L}$ gauge groups, respectively. For the generation of SM quark and lepton masses through a universal seesaw, the model includes heavy singlet quarks

$$U_L(3, 1, 1, \frac{4}{3}),\ U_R(3, 1, 1, \frac{4}{3}),\\ D_L(3, 1, 1, -\frac{2}{3}),\ D_R(3, 1, 1, -\frac{2}{3});$$

singlet charged leptons

$$E_L(1, 1, 1, -2),\ E_R(1, 1, 1, -2);$$

and singlet heavy neutrinos

$$N_L(1, 1, 1, 0),\ N_R(1, 1, 1, 0).$$

[1] We shall refer to these heavy Majorana neutrinos as "heavy neutrinos" in the remainder of the text.

Table 1 Particle spectrum along with their quantum numbers

Field	$SU(3)_C$	$SU(2)_L$	$SU(2)_R$	$U(1)_{B-L}$	Z_2
$Q_{L(R)} = \begin{pmatrix} u \\ d \end{pmatrix}_{L(R)}$	3	2 (1)	1 (2)	$\frac{1}{3}$	+
$l_{L(R)} = \begin{pmatrix} \nu \\ e \end{pmatrix}_{L(R)}$	1	2 (1)	1 (2)	-1	+
U_L, U_R	3	1	1	$\frac{4}{3}$	+
D_L, D_R	3	1	1	$-\frac{2}{3}$	+
E_L, E_R	1	1	1	-2	-
N_L, N_R	1	1	1	0	-
$H_{L(R)Q} = \begin{pmatrix} H^+ \\ H^0 \end{pmatrix}_{L(R)Q}$	1	2 (1)	1 (2)	1	+
$H_{L(R)l} = \begin{pmatrix} H^+ \\ H^0 \end{pmatrix}_{L(R)l}$	1	2 (1)	1 (2)	1	-

The Higgs sector consists of four $SU(2)$ doublets:

$$H_{RQ}(1,1,2,1) = \begin{pmatrix} H^+_{RQ} \\ H^0_{RQ} \end{pmatrix}, \quad H_{LQ}(1,2,1,1) = \begin{pmatrix} H^+_{LQ} \\ H^0_{LQ} \end{pmatrix},$$
$$H_{Rl}(1,1,2,1) = \begin{pmatrix} H^+_{Rl} \\ H^0_{Rl} \end{pmatrix}, \quad H_{Ll}(1,2,1,1) = \begin{pmatrix} H^+_{Ll} \\ H^0_{Ll} \end{pmatrix}. \tag{6}$$

Under the Z_2 symmetry, the singlet leptons E_L, E_R, N_L, N_R, and the lepton specific scalar doublets H_{Ll} and H_{Rl} are odd, while the rest are all even. The Z_2 charge assignments allow the H_{LQ} and H_{RQ} to interact specifically with quarks, while H_{Ll} and H_{Rl} only have leptonic interactions. The neutral components of the two $SU(2)_{R/L}$ Higgs doublets acquire non-zero vacuum expectation values (VEV) to break the LRSM symmetry down to $U(1)_{\rm QED}$. The VEVs are given as

$$\left\langle H^0_{RQ} \right\rangle = v_{RQ}/\sqrt{2}, \quad \left\langle H^0_{Rl} \right\rangle = v_{Rl}/\sqrt{2},$$
$$\left\langle H^0_{LQ} \right\rangle = v_{LQ}/\sqrt{2}, \quad \left\langle H^0_{Ll} \right\rangle = v_{Ll}/\sqrt{2} \tag{7}$$

with the constraint $v^2_{LQ} + v^2_{Ll} = v^2_{EW}$, where $v_{EW} = 246$ GeV is the electroweak (EW) vacuum expectation value. The hierarchy of the VEVs is arranged as

$$v_{RQ}, v_{Rl} >> v_{LQ} > v_{Ll}. \tag{8}$$

The VEVs of the $SU(2)_R$ scalar doublets, v_{RQ} and v_{Rl}, are responsible for generating the mass of W_R and Z_R gauge bosons, while the VEVs to the $SU(2)_L$ scalar doublets,v_{LQ} and v_{Ll}, break the EW symmetry and generate the SM gauge boson (W and Z) masses.

The full Lagrangian of this model can be written as

$$\mathscr{L} = \mathscr{L}_{kinetic} + \mathscr{L}_Y + V(H), \tag{9}$$

where $\mathscr{L}_{kinetic}$ contains the kinetic terms for the gauge boson, scalars and fermions in the model, while the Yukawa Lagrangian, $\mathscr{L}_Y$ and the scalar potential, $V(H)$ are given later in Eqs. (14) and (21), respectively.

The covariant derivatives appearing in $\mathscr{L}_{kinetic}$ can be written as,

$$\mathscr{D}_\mu Q_{L/R} = \left[\partial_\mu - i\frac{g_{L/R}}{2}\tau.W_{L/R\mu} - i\frac{g_V}{6}V_\mu\right] Q_{L/R},$$
$$\mathscr{D}_\mu l_{L/R} = \left[\partial_\mu - i\frac{g_{L/R}}{2}\tau.W_{L/R\mu} + i\frac{g_V}{2}V_\mu\right] l_{L/R},$$
$$\mathscr{D}_\mu H_{L/R} = \left[\partial_\mu - i\frac{g_{L/R}}{2}\tau.W_{L/R\mu} - i\frac{g_V}{2}V_\mu\right] H_{L/R}, \tag{10}$$

where V_μ is the $U(1)_{B-L}$ gauge boson and g_V its gauge coupling, while W_L, W_R and g_L, g_R are the gauge bosons and gauge couplings corresponding to the $SU(2)_L$ and $SU(2)_R$ gauge groups, respectively. The mass of the charged gauge bosons W_R and W_L are given by

$$M^2_{W^\pm_R} = \frac{1}{4}g^2_R(v^2_{RQ}+v^2_{Rl}), \quad M^2_{W^\pm} = \frac{1}{4}g^2_L(v^2_{LQ}+v^2_{Ll}). \tag{11}$$

The masses of the two neutral massive gauge bosons are given by

$$M^2_{Z_R} \simeq \frac{1}{4}\left[(g^2_R + g^2_V)(v^2_{RQ} + v^2_{Rl}) + \frac{g^4_V(v^2_{LQ} + v^2_{Ll})}{g^2_R + g^2_V}\right],$$
$$M^2_Z \simeq \frac{1}{4}(g^2_L + g^2_Y)(v^2_{LQ} + v^2_{Ll}) \tag{12}$$

in the limit $v_{EW} << v_{RQ}, v_{Rl}$. Here, g_Y is the effective SM $U(1)_Y$ gauge coupling given as

$$g_Y = \frac{g_L g_V}{\sqrt{g^2_L + g^2_V}}. \tag{13}$$

In this model, the Z_R is always heavier than W_R, which implies that a strong limit on W_R mass indirectly puts a

stronger bound on Z_R mass. We discuss the generation of masses for the fermions through the seesaw mechanism in the the following subsection.

2.1 Seesaw and fermion masses

The quarks and leptons obtain their masses through a universal seesaw with the help of heavy singlet fermionic states. The Lagrangian in this model contains the following gauge invariant Yukawa terms:

$$\begin{aligned}\mathscr{L}_Y = &(Y_{uL}\overline{Q}_L\widetilde{H}_{LQ}U_R + Y_{uR}\overline{Q}_R\widetilde{H}_{RQ}U_L + Y_{dL}\overline{Q}_L H_{LQ}D_R\\ &+Y_{dR}\overline{Q}_R H_{RQ}D_L + Y_{\nu L}\bar{l}_L\widetilde{H}_{Ll}N_R + Y_{\nu R}\bar{l}_R\widetilde{H}_{Rl}N_L\\ &+Y_{eL}\bar{l}_L H_{Ll}E_R + Y_{eR}\bar{l}_R H_{Rl}E_L + M_U\overline{U}_L U_R\\ &+M_D\overline{D}_L D_R\\ &+ M_E\overline{E}_L E_R + M_N\overline{N}_L N_R + H.C.)\\ &+M_L N_L^T N_L^C + M_R N_R^T N_R^C. \end{aligned} \tag{14}$$

Here, Y_{iA}'s are the Yukawa coupling matrices, and M_X's are the heavy singlet mass terms. The $\widetilde{H}_{L/R}$ is the conjugate scalar defined as

$$\widetilde{H}_{L/R} = i\tau_2 H^*_{L/R}. \tag{15}$$

All the charged fermions, i.e., quarks and charged leptons, acquire their masses by diagonalizing 6×6 matrices through a universal seesaw mechanism. Three light eigenstates among the six eigenstates are identified as the three SM states.

The up quarks acquire their masses from the following mass matrix

$$M_u = \begin{pmatrix} 0 & Y_{uR}v_{RQ}/\sqrt{2} \\ Y_{uL}^T v_{LQ}/\sqrt{2} & M_U \end{pmatrix} \tag{16}$$

in the (u, U) basis. This matrix is diagonalized by the following bi-unitary transformation:

$$M_u^{diag} = U_{uL}M_u U_{uR}^\dagger, \tag{17}$$

where U_{uL} and U_{uR} are 6×6 unitary matrices transforming the left-handed and right-handed fermions from the gauge basis to their mass basis. The down quarks also acquire their masses through the seesaw mechanism, where the corresponding matrices are U_{dL} and U_{dR}. For simplicity, we choose the $Y_{uL/R}$ and Y_{dR} to be diagonal and keep only Y_{dL} to be off-diagonal so as to generate the correct Cabibbo–Kobayashi–Maskawa (CKM) mixing matrix for the SM quarks. The 6×6 mixing matrix

$$U_L^{CKM} = U_{uL}U_{dL}^\dagger \tag{18}$$

contains the SM CKM matrix in the *top-left* (*bottom-right*) 3×3 block if mass eigenvalues are arranged in ascending (descending) order. The mixing between the SM light quarks and the heavy quarks is negligible except for the top quark as it is heavy.

The charged leptons acquire their masses from the following 6×6 mass matrix:

$$M_e = \begin{pmatrix} 0 & Y_{eR}v_{Rl}/\sqrt{2} \\ Y_{eL}^T v_{Ll}/\sqrt{2} & M_E \end{pmatrix}. \tag{19}$$

The Yukawa coupling matrices ($Y_{eL/R}$) and the heavy lepton mass matrix (M_E) are chosen diagonal to prevent any charged lepton flavor violating interactions. The hierarchical structure of the block matrices that give the correct masses to the SM charged leptons ($e,\ \mu,\ \tau$) allow negligible mixing between the SM charged leptons and heavy charged leptons.

The neutrinos obtain their masses from the following 12×12 mass matrix:

$$\begin{pmatrix} 0 & Y_{\nu L}v_{Ll}/\sqrt{2} & 0 & 0 \\ Y_{\nu L}^T v_{Ll}/\sqrt{2} & M_R & 0 & M_N^T \\ 0 & 0 & 0 & Y_{\nu R}^T v_{Rl}/\sqrt{2} \\ 0 & M_N & Y_{\nu R}v_{Rl}/\sqrt{2} & M_L \end{pmatrix} \tag{20}$$

formed in the basis $(\nu_L^*, N_R, \nu_R, N_L^*)$.

Similar to the quark sector, all the Yukawa couplings and mass matrices are taken diagonal except $Y_{\nu L}$ that generates the Pontecorvo–Maka–Nakagawa–Sakata (PMNS) mixing matrix [4].

2.2 Scalar masses

The scalars obtain their masses by minimizing the following gauge-invariant potential

$$\begin{aligned} V(H) = &\sum_{i=1}^{4}\mu_{ii}H_i^\dagger H_i + \sum_{\substack{i,j=1\\ i\le j}}^{4}\lambda_{ij}H_i^\dagger H_i H_j^\dagger H_j\\ &+\Big[\alpha_1 H_{LQ}^\dagger H_{Ll}H_{RQ}^\dagger H_{Rl} + \alpha_2 H_{LQ}^\dagger H_{Ll}H_{Rl}^\dagger H_{RQ}\\ &+\mu_{12}^2 H_{LQ}^\dagger H_{Ll} + \mu_{34}^2 H_{RQ}^\dagger H_{Rl} + H.C.\Big], \end{aligned} \tag{21}$$

where

$$H_1 = H_{LQ},\quad H_2 = H_{Ll},\quad H_3 = H_{RQ},\quad H_4 = H_{Rl}. \tag{22}$$

The terms μ_{12} and μ_{34} break the discrete Z_2 symmetry softly and prevent the formation of domain walls which could otherwise destabilize the model [34,35].

The Higgs boson spectrum consists of four CP-even states, two CP-odd states, and two charged Higgs bosons. A major distinctive feature from the more widely studied minimal LRSM model which includes scalar triplets, is the absence of a doubly charged Higgs boson in the particle spectrum of our model. Two charged goldstone bosons are eaten

up by the W_L and W_R gauge bosons to give them mass, while two neutral goldstone states provide mass to the Z and Z_R.

3 Phenomenological benchmark points

We now highlight some of the constraints on the parameter space in our model before discussing the choice of our benchmark points for the collider analysis. We note that the most relevant constraints arise from the experimental bound on heavy gauge boson masses. We also mention a few theoretical constraints that affect our parameter choices.

3.1 Theoretical and phenomenological constraints

The theoretical constraints on some of the couplings in the model come from the requirement of perturbativity and unitarity. The perturbativity condition requires that at least at the electroweak symmetry breaking (EWSB) scale, all quartic couplings satisfy

$$C_{H_i H_j H_k H_l} < 4\pi, \tag{23}$$

whereas the Yukawa and gauge couplings need to be less than $\sqrt{4\pi}$ [36]. Furthermore, tree-level unitarity in the scattering of Higgs bosons and longitudinal components of EW gauge bosons necessitates that the eigenvalues of the scattering matrices must be less than 16π [37,38].

Additional constraints appear as a result of electroweak precision measurements, particularly the oblique parameters [39]. The addition of extra Higgs doublets has little effect on the oblique parameter in general, particularly the T-parameter because the custodial $SU(2)$ stays intact at the tree level. It can be broken at the loop level by the effect of other states. However, the additional states in our model primarily belong to the right-handed sector and are rather heavy. Although the mixing between the left and right sectors is tiny, it cannot cause significant changes in the EW W or Z boson masses. The consistency of our chosen benchmarks has been checked against existing limits [40].

3.2 Experimental constraints

The non-observation of any direct signal at the LHC has put stringent constraints on the mass of the heavy right-handed gauge bosons Z_R, W_R as well as the heavy Majorana neutrinos in LRSM. The different constraints leading to limits on the model are briefly summarized below.

Searches for heavy resonances:

The search for heavy resonances decaying to di-lepton/di-jet final state at the LHC put strong constraints on their production cross section. The major experimental constraint in our model comes from the W_R search in the $l^{\pm}N$ channel (N represents the heavy right-handed neutrino) where the final state is either one charged lepton and a fatjet containing a high P_T lepton [43] or two same-sign leptons and two jets [44,45], depending on the mass difference of W_R and N. The most recent CMS search [41] puts a lower limit on W_R which excludes its masses below 4.7 TeV and 5.0 TeV for the electron ($e^{\pm}$) and muon ($\mu^{\pm}$) channels, respectively. On the other hand, ATLAS [42] di-jet search puts a lower bound of 4 TeV on W_R mass with SM-like couplings (i.e., 50% branching in di-jet mode). These limits differ depending on the branchings of W_R in the di-jet and the $l^{\pm}N$ channels. These dependencies are summarized in Fig. 6 of Ref. [41] and Fig. 4c of Ref. [42], and one can extract the bound on M_{W_R} depending on the value of production cross sections times the branching ratios. Both the CMS [41] and ATLAS [43] collaborations have used the minimal LRSM (MLRSM) model in their search for the heavy W_R boson, where the $W_R \to eN$ decay branching ratio is about 10% for large values of the W_R mass [46]. In our case, the branching ratio is relatively smaller ($< 5\%$) due to new modes of decay available for the W_R boson into heavy leptons (seesaw partners) and heavy neutrinos, as shown in Table 4. As the decay branching ratio of $W_R \to eN$ is suppressed, limits on the W_R mass are relaxed (see *left-panel* of Fig. 1) when compared to the CMS [41] 4.7 TeV bound in the electron channel. In the di-jet mode, one notes that the branching for W_R is 66% in our model, and thus the limit on W_R mass increases (see *right-panel* of Fig. 1). We have a common limit of 4.3 TeV on W_R mass coming either from $l^{\pm}N$ or di-jet search for our parameter choices.

The heavy neutral gauge boson (Z_R) has a rather weak limit from the direct di-jet search [47] excluding $m_{Z_R} < 2.9$ TeV having SM-like gauge couplings with the SM fermions. However, in LRSM the Z_R is heavier than W_R, and thus a strong limit on W_R mass indirectly puts a stronger limit on Z_R mass (see Eqs. (11) and (12)). The 4.3 TeV lower limit on W_R mass, as discussed above, puts a lower limit of 5 TeV on Z_R mass.

In addition, we have also considered heavy neutrino search results from the LHC which put limits on m_N [44,48,49], and these are included in our benchmark selection.

Bounds from FCNC and Higgs searches: We avoid flavor-violating interactions of charged leptons with neutral scalars by choosing diagonal configurations for the corresponding Yukawa matrices involving the SM and heavy exotic leptons. There are no flavor-changing neutral Higgs (FCNH) interactions in our model at the tree-level because of the diagonal couplings for the neutral scalars. Heavy non-standard neutral scalars, pseudoscalars and the charged Higgses have strong bounds [50,51] from low energy flavour-changing neutral current (FCNC) effects, especially from the K-meson and B-meson mass mixing. These bounds have been studied for the MLRSM in Ref. [52]. As the FCNH effects are absent,

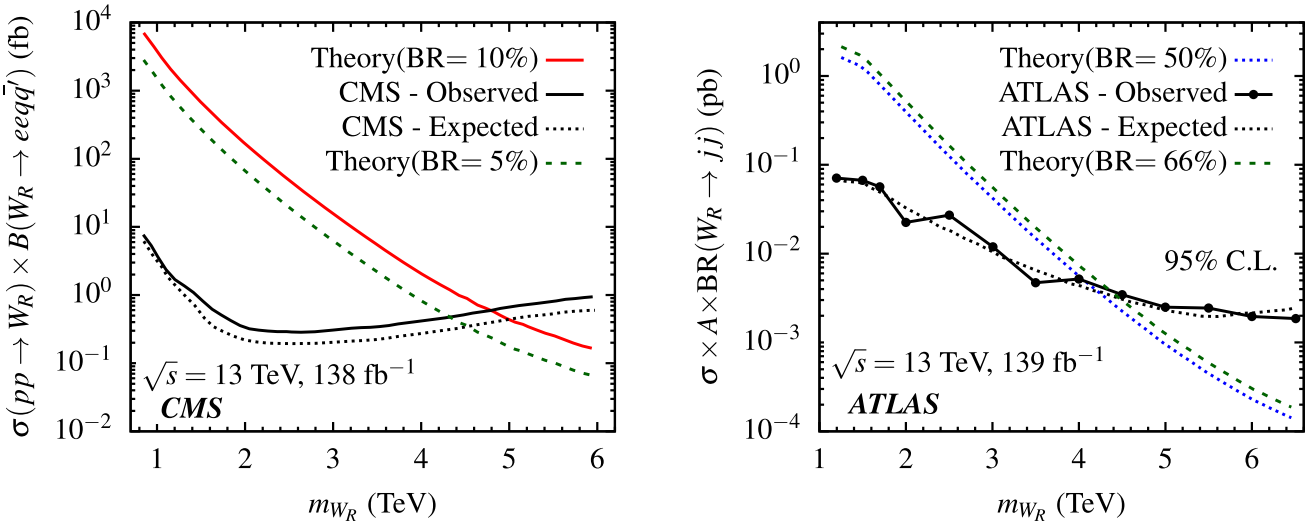

Fig. 1 Limit for the cross section times the branching ratio of W_R as a function of its mass at 95% CL are shown from CMS heavy neutrino search [41] (left-panel) and ATLAS dijet search [42] (right-panel). Theoretical expectations for the cross sections are also shown with the branching ratios used in the experimental search (10% in left-panel and 50% in right panel) and in our analysis (5% in left-panel and 66% in right- panel). Please refer to the text for more details

these bounds do not apply on our neutral states. The W_R mass limits coming from the meson mixings are much weaker than the direct collider bounds.

The signal intensity measurements of the 125 GeV Higgs in several final states, including ZZ, WW, bb, $\tau\tau$, and $\gamma\gamma$ final states [53,54], provide additional constraints, which have been considered while choosing our benchmark points. The gauge and Yukawa couplings of the 125 GeV scalar seem to lie extremely close to their SM value, as suggested by the experimental results. We thus limit our study to the alignment limit, i.e., $|y_h^V| \sim 1$, which is the modification factor to the hVV ($V = W/Z$) couplings due to new physics. The parameter space of interest is further restricted by collider searches for non-standard neutral scalar states and charged scalar states. These searches are carried out at the LHC [55–59] in a variety of SM final states limiting their masses in the range of 1–2 TeV. As our non-standard neutral and charged scalar states are considered to be very heavy they do not affect our analysis.

3.3 Chosen parameter space

Motivated by the signal of fatjet searches arising from heavy vector-like leptons and heavy neutrinos, we choose the heavy charged lepton mass to be $\sim$ 0.72–1 TeV while three heavy neutrino masses in the range of $\sim$ 180–700 GeV and $m_{W_R} \approx$ 4.5–5 TeV, which are consistent with all experimental observations. The remaining BSM particles, including heavy Higgs (charged and neutral), pseudoscalar, heavy quarks, and the remaining six heavy neutrinos, are kept at very high mass ($>$ 5 TeV), which does not contribute to the collider signatures considered in this article. We choose three benchmark points (BP) having $m_{W_R} = 4.5$ in BP1 and $m_{W_R} = 5$ TeV in BP2 and BP3. For BP3, we further subdivide the benchmark through one heavy charged mass. The heavy charged leptons are kept around 1 TeV in BP1 and BP2 (low boost), while they are kept around 0.72 TeV in BP3 (high boost). The scalar and gauge boson masses are shown in Table 2 for the three benchmark points. In Table 3, we show fermion masses chosen for our phenomenological study.

All the Yukawa matrices in Eq. (14) are chosen diagonal except the Y_{dL} and $Y_{\nu L}$ to generate experimentally measured CKM parameters and neutrino mixing matrix U_{PMNS} as discussed before. The diagonal heavy singlet fermion (quark and lepton) mass matrices are taken to be

$$\begin{aligned} M_U &= \mathrm{Diag}\,(30.0, 11.93, 6.6) \times 10^3, \\ M_D &= \mathrm{Diag}\,(1.6, 2.0, 3.0) \times 10^4, \\ M_E &= \mathrm{Diag}\,(0.8, 1.0, 1.0) \times 10^3, \\ M_R &= M_L = \mathrm{Diag}\,(1.0, 1.0, 1.0) \times 10^4, \\ M_N &= \mathrm{Diag}\,(1.0, 1.0, 1.0) \times 5 \times 10^3 \end{aligned} \tag{24}$$

in units of GeV. These inputs for the singlets with appropriate Yukawa coupling matrices produce the desired mass of SM fermions together with the heavy fermion eigenstates shown in Table 3. The Yukawa couplings are chosen as

$$\begin{aligned} &Y^{11}_{u(L,R)} \sim Y^{11}_{d(L,R)} \sim Y^{11}_{e(L,R)} \simeq 10^{-2}, \\ &Y^{22}_{u(L,R)} \sim Y^{22}_{dR} \sim Y^{22}_{e(L,R)} \simeq 10^{-1}, \\ &Y^{33}_{u(L,R)} \sim Y^{33}_{dL} \sim Y^{33}_{eR} \simeq 1.0. \end{aligned} \tag{25}$$

Table 2 Gauge boson and scalar masses with the common input parameters $\alpha_1 = -0.2$, $\alpha_2 = 0.1$, $\lambda_{11} = 0.1307$, $\lambda_{12} = 0.8$, $\lambda_{13} = 0.05$, $\lambda_{14} = -0.1$, $\lambda_{22} = 0.5$, $\lambda_{23} = 0.1$, $\lambda_{24} = 0.1$, $\lambda_{33} = 0.2$, $\lambda_{34} = 0.1$, $\lambda_{44} = 0.1$, $\mu_{12}^2 = -2.5 \times 10^4$, $\mu_{34}^2 = -8.5 \times 10^7$, $v_{LQ}/\sqrt{2} = 173.4$ GeV, $v_{Ll}/\sqrt{2} = 14$ GeV. The right handed VEVs for BP1 are $v_{RQ} = 10.6$ and $v_{Rl} = 8.4$ TeV, and that for BP2 and BP3 are $v_{RQ} = 12.48$ TeV and $v_{Rl} = 8.4$ TeV

Particle	Mass	
	BP1	BP2 and BP3
W_R	4.5 TeV	5.0 TeV
Z_R	5.33 TeV	5.93 TeV
H_1	125.8 GeV	126.0 GeV
H_2	6.38 TeV	7.4 TeV
H_3	7.51 TeV	8.15 TeV
H_4	13.89 TeV	14.31 TeV
A_1	7.51 TeV	8.15 TeV
A_2	13.2 TeV	13.52 TeV
H_1^+	7.51 TeV	8.15 TeV
H_2^+	13.2 TeV	13.52 TeV

We require $Y_{dR}^{33} \simeq 0.092(0.078)$ in BP1 (BP2 and BP3); $Y_{eL}^{33} \simeq 0.146(0.132)$ in BP1 and BP2 (BP3) to keep the third generation heavy fermion masses in few TeV range. We set the off-diagonal elements in Y_{dL} matrix by fitting them to get the experimentally measured CKM mixing matrix [60] within 4σ error, with $Y_{dL}^{21} = Y_{dL}^{32} = Y_{dL}^{31} = 0$. The values of Y_{dL}^{12}, Y_{dL}^{13}, and Y_{dL}^{23} are shown in Fig. 2 in *left-panel* for different scanning configurations (horizontal axis) in BP1. The values are $|Y_{dL}^{12}| \simeq 10^{-3}$, $|Y_{dL}^{13}| \simeq 3 \times 10^{-3}$, and $|Y_{dL}^{23}| \simeq 4 \times 10^{-2}$ for all scanning configuration. The values of Y_{dL}^{12}, Y_{dL}^{13}, and Y_{dL}^{23} are of the same order of magnitude as above, for all our benchmark points.

Similar to the quark sector Yukawa, we keep the $Y_{\nu R}$ diagonal while $Y_{\nu L}$ is chosen non-diagonal in order to obtain the neutrino mixing matrix U_{PMNS}. We choose $Y_{\nu R} =$ Diag (0.2, 0.3, 0.4) and scan the parameter space for $Y_{\nu L}^{ij}$ which is shown in Fig. 2 in the *right-panel* with different scanned configurations (horizontal axis) which satisfy 6.82×10^{-5} eV^2 $< \Delta m_{21}^2 < 8.04 \times 10^{-5}$ eV^2, 2.43×10^{-3} eV^2 $< \Delta m_{31}^2 < 2.60 \times 10^{-3}$ eV^2 and U_{PMNS} mixing

Table 3 The heavy quarks, charged and neutral lepton masses for the benchmark points with the input parameters shown in Eqs. (24) and (25)

Up-type quark (TeV)	Down-type quark (TeV)	Charged lepton (TeV)		Neutrino (GeV)	(TeV)
BP1, BP2, BP3	BP1, BP2, BP3	BP1, BP2	BP3	BP1, BP2, BP3	
$m_U = 11.94$	$m_D = 16.0$	$m_{E_4} = 1.17$	0.721	$m_{\nu_4} = 186.0$	$m_{\nu_7} = 5.14$
$m_C = 11.96$	$m_S = 20.1$	$m_{E_5} = 2.0$	1.3	$m_{\nu_5} = 404.8$	$m_{\nu_8} = 5.30$
$m_T = 30.0$	$m_B = 30.0$	$m_{E_6} = 2.56$	1.87	$m_{\nu_6} = 689.7$	$m_{\nu_9} = 5.50$
					$m_{\nu_{10}} = 15.05$
					$m_{\nu_{11}} = 15.11$
					$m_{\nu_{12}} = 15.19$

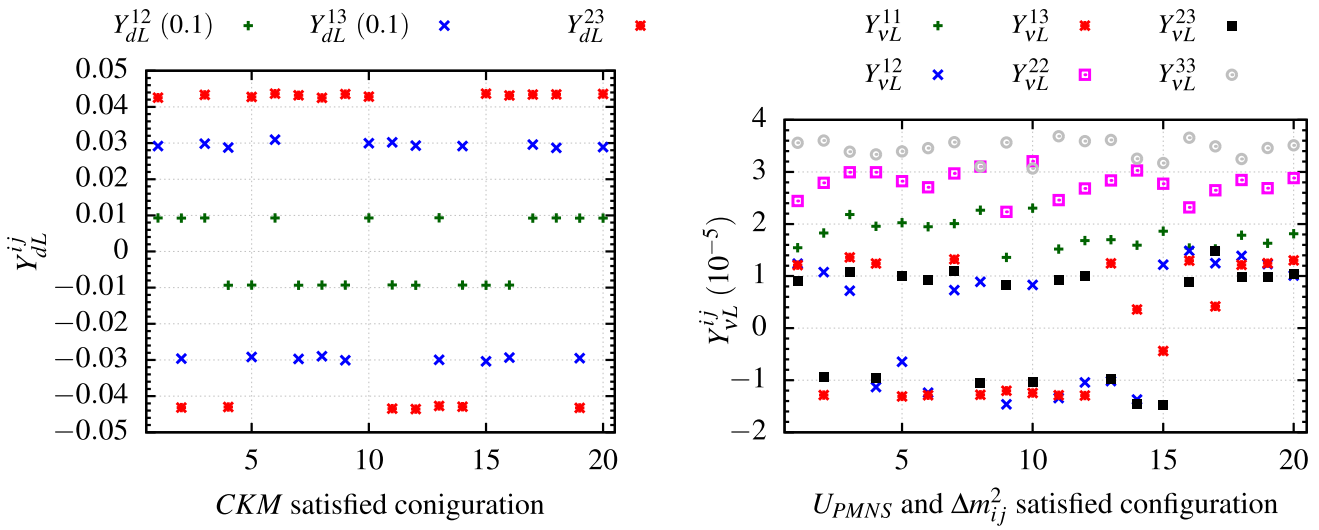

Fig. 2 The CKM satisfied points for the Y_{dL}, and the U_{PMNS} and Δm_{ij}^2 satisfied points for the $Y_{\nu L}$ are shown in the left-panel and right-panel, respectively for BP1

elements within 3σ error [4,5]. The relative values of $Y_{\nu L}^{ij}$ are below 4×10^{-5} keeping the relative order intact among themselves. We have chosen the first point in the scanned configuration in our analysis.

4 Collider analysis

In this section, we study the collider signatures of our model at the high luminosity run of the LHC with the chosen benchmark parameters discussed above. Even though the exotic charged and neutral leptons are very heavy and have very limited production rates through SM gauge bosons, they can be resonantly produced through the heavy $SU(2)_R$ gauge bosons with comparatively large rates. We therefore focus on the production of heavy neutrinos and heavy charged leptons through the s-channel processes mediated by the heavy right-handed gauge bosons. Once produced, these heavy charged leptons (E_i's) and neutrinos (ν_i, where $i \geq 4$) finally decay to SM leptons and jets with almost 100% branching ratios, as shown in Table 4 for `BP1`. The branching ratios for the other benchmark points, viz. `BP2` and `BP3` are shown in Table 12 in the Appendix A. The decay of these heavy fermions (produced from the decay of very heavy $SU(2)_R$ gauge bosons) leads to the interesting possibility of final states with boosted objects. What we finally observe are some clusters of highly boosted and collinear particles, which can only be detected as a large radius jet in the detector. The presence of these fatjets play an important role in achieving good signal significance over the estimated SM background. In addition, the fatjet from the decay of heavy charged lepton also contains a non-isolated SM charged lepton along with two sub-jets. The fatjet originating from the heavy neutrino decay contains two sub-jets, as shown in Eq. (1). In our work, we therefore look for fatjets containing charged leptons and analyze these fatjets by studying their *substructure*. We consider signals with different fatjet multiplicities, that include inclusive two, three, and four fatjets. Note that our primary production channel involves particles (E_i and ν_i) that carry a lepton number which leads to some of the fatjets having a non-isolated charged lepton (e, μ) within the fatjet radius. We use the jet-substructure techniques [33] to identify the sub-jet associated with these boosted charged leptons when they cannot be isolated at the detector.

Table 4 The relevant branching ratios are listed for the decay channel of the heavy gauge bosons W_R and Z_R, heavy leptons E_i, and lightest three heavy neutrinos ν_i, ($i = 4, 5, 6$) in `BP1`

Decay	Branching
$W_R^+ \to jj$	66.0%
$W_R^+ \to t\bar{b}$	10.2%
$W_R^+ \to e^+\nu_4$	5.03 %
$W_R^+ \to \mu^+\nu_5$	1.58 %
$W_R^+ \to \tau^+\nu_6$	2.43 %
$W_R^+ \to E_4^+\nu_4$	5.16 %
$W_R^+ \to E_5^+\nu_6$	5.08 %
$W_R^+ \to E_6^+\nu_5$	4.60 %
$Z_R \to jj$	47.5%
$Z_R \to \nu_4\nu_4$	7.17%
$Z_R \to \nu_5\nu_5$	6.56%
$Z_R \to E_4\bar{E}_4$	2.23%
$Z_R \to E_5\bar{E}_5$	1.15%
$E_4 \to \nu_4 jj$	70.6%
$E_5 \to \nu_6 jj$	8.68%
$E_6 \to \nu_5 jj$	73.7%
$E_6 \to \mu jj$	3.65%
$\nu_4 \to e^\pm jj$	100%
$\nu_5 \to \mu^\pm jj$	94.5%
$\nu_6 \to \tau^\pm jj$	87.3%

4.1 Signal and background

Here we describe the fatjet signals we are interested in, followed by the possible SM background in detail. We have generated events for all our signal and background processes using `MadGraph5_aMC@NLO` v2.7.3 [61] at leading order (LO) in QCD with a dynamic choice of factorization scale given by $\sum M_i^T/2$, where M_i is the transverse mass of final state particles. We use `nn23lo1` [62] for the parton distribution functions (PDFs). Events are passed to `PYTHIA8` [63] for showering and hadronization followed by a fast detector simulation in `Delphes v3.4.2` [64], with added pile-up events embedded in `Delphes v3.4.2` for the high luminosity LHC (HL-LHC). The final state hadrons with non-isolated high P_T leptons are clustered using the Cambridge-Aachen algorithm of `FastJet` [65,66] with a jet radius $R_0 = 0.8$ (AK8 fatjet). We groom [67] the fatjets using soft-drop method [68,69] to remove soft and wide angle radiations after some pre-selection cuts. We use the soft radiation fraction parameter $z_{cut} = 0.1$ and the angular exponent parameter $\beta = 0$ for the grooming [41]. The groomed AK8 fatjets are required to have a threshold on the soft-drop mass (m_{SD}) as $m_{SD} > 40$ GeV.

To identify the sub-jets associated with leptons and leading hadrons we employ the N-subjettiness technique, where we use 'OnePass General ET General KT Axes' with $p = 0.6$ (for kt and Cambridge-Aachen axis choice of $p = 1$ and $p = 0$, respectively) [70,71]. To use this method for finding sub-jets out of a fatjet, we use `Fastjet Contrib` [72]. The $t\bar{t}$ background was estimated at next-to-next LO (NNLO) using a k-factor of 1.6 [73].

4.1.1 Fatjet signals

We consider three types of signals containing fatjets for our analysis which are described below. Note that all the signal fatjets have $P_T > 200$ GeV before grooming. This pre-selection cut on the reconstructed fatjets is imposed to suppress the SM background, especially the large QCD multijet background. As we wish to study the signal which dominantly comes from the production of the heavy $SU(2)_R$ gauge bosons which have masses above 5 TeV, the fatjets originating from them are expected to have significantly large P_T. This pre-selection helps in removing the background contributions without compromising on the signal events. *Two fatjet inclusive searches* In this signal topology, our final state contains at least two high P_T fatjets, with each containing one high P_T lepton lying inside the fatjet radius. The five different production channels that contribute to this final state in our model are

i. **Signal 1:** $pp \to W_R,\ W_R \to E_4\nu_4,\ E_4 \to \nu_4 jj$ (both the ν_4 then decay into e/μ with additional two jets),
ii. **Signal 2:** $pp \to W_R,\ W_R \to E_6\nu_5,\ E_6 \to \nu_5 jj$ (both ν_5 will then decay into e/μ with additional two jets),
iii. **Signal 3:** $pp \to W_R,\ W_R \to E_6\nu_5,\ E_6 \to \mu jj$ (ν_5 then decays into e/μ with additional two jets),
iv. **Signal 4:** $pp \to Z_R,\ Z_R \to (\nu_4\nu_4)/(\nu_5\nu_5)$ (ν_4/ν_5 then decay into e and μ with additional two jets),
v. **Signal 5:** $pp \to Z_R,\ Z_R \to E_4\bar{E}_4,\ E_4 \to \nu_4 jj$ (ν_4 then decays into e/μ with additional two jets).

Three-fatjet inclusive searches Here our final state contains at least three high P_T fatjets, where the two leading (P_T-ordered) fatjets must contain one high P_T lepton in them. The three production channels that dominantly contribute to this three-fatjet signal are given by

i. **Signal 1:** $pp \to W_R,\ W_R \to E_4\nu_4,\ E_4 \to \nu_4 jj$ (all ν_4 then decay into e/μ with additional two jets), a representative Feynman diagram for this channel is shown in Fig. 3,
ii. **Signal 2:** $pp \to W_R,\ W_R \to E_6\nu_5,\ E_6 \to \nu_5 jj$ (both the ν_5 then decay into e/μ with additional two jets),
iii. **Signal 3:** $pp \to Z_R,\ Z_R \to E_4\bar{E}_4,\ E_4 \to \nu_4 jj$ (each ν_4 then decays into e/μ with additional two jets).

Four-fatjet inclusive searches In this signal, the final state contains at least four high P_T fatjets with the leading two fatjets inclusive of only one high P_T lepton within their jet radius. For this case we find that only $pp \to Z_R,\ Z_R \to E_4\bar{E}_4,\ E_4 \to \nu_4 jj$ contributes dominantly where ν_4 as before decays into $e/\mu + jj$.

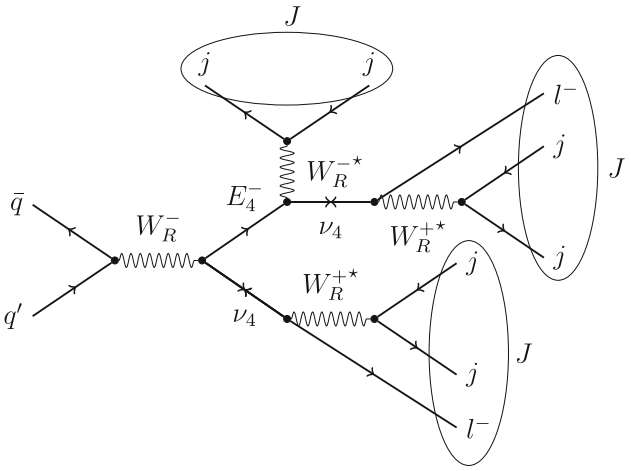

Fig. 3 Representative Feynman diagram for three fatjet signal

All individual contributions in the respective final states are summed together and identified as the $signal$.

4.1.2 Backgrounds

For the above signals, we consider the following SM background. *QCD multi-jet:* QCD multi-jet events will be a major source of background due to its large production cross section. We primarily focus on the 4-jet final state, which can lead to our two, three, or four fatjet signals where some jet could also fake a lepton as a part of the fatjet. We however find that a large P_T cut on the fatjet and a cut on the jet invariant mass helps to reduce the QCD background by a significant amount. *Top pair production* ($t\bar{t}$): The other dominant background for our signal comes from the SM production of $t\bar{t}$ where the leptonic decay mode of $t\bar{t}$ can give us fatjets with two high P_T lepton as part of the fatjets. On the other hand, the semi-leptonic and fully hadronic decay mode of $t\bar{t}$ can also be a dominant background where one or two hadrons can fake as leptons or have leptonic decays in the detector. *W/Z+jets and tW*: The weakly produced ZW and tW processes can also be possible sources of fatjet background. However, the production cross section of both these processes are very small compared to the QCD and $t\bar{t}$ background. In addition, for the tW case the probability of getting at least two heavy and highly boosted fatjets is much smaller than $t\bar{t}$ due to the lower mass of W. The other SM subprocesses that can give fatjet signatures are W/Z+jets. Although the production cross section for W/Z+jets is comparatively much larger than tW, it has less probability of giving at least two high-energy leptons in two separate fatjets, when compared to the $t\bar{t}$ leptonic decay case.

We therefore, neglect the above backgrounds in our analysis.

4.2 Variables

To achieve good signal significance over the aforementioned backgrounds, we identify some kinematic variables which have characteristically different distributions for the signal compared to the SM background.

After analyzing various distributions, we find the relevant variables to be the P_T and invariant mass of the fatjets, P_T of the sub-jets associated with leptons, and two interesting substructure variables LSF and LMD.

The P_T-ordered jets and the jet-mass are denoted by $P_{T\,j_i}$ and m_{j_i} where $i = 1, 2, 3, 4$.

The invariant mass of any two, three, and four fatjets are also important variables and are called $m_{j_1 \ldots j_n}$. In addition, we include two jet substructure variables that have been used for fatjet analyses in CMS searches [41], viz. the lepton sub-jet fraction (LSF) and lepton mass drop (LMD) of the sub-jet associated with charged leptons [33].

To compute the variables LSF and LMD, we cluster all final state particles in the event (including leptons) into a fatjet. For each fatjet we then use jet-substructure (JSS) algorithms to cluster its constituents in three sub-jets using N-subjettiness techniques [72]. We then check for sub-jets associated with all high P_T leptons. Thereafter we calculate the lepton sub-jet fraction of each lepton (defined as the ratio between the lepton P_T and P_T of the sub-jet associated with it) which is given by

$$LSF_n = \frac{P_{T\,l_n}}{P_T{}^{sj}_{l_n}} \tag{26}$$

where $n = 1, 2$. LSF_1 is associated with the leading lepton while LSF_2 is for the sub-leading one. The lepton mass drop parameter is constructed in a similar way and given by

$$LMD_n = \frac{m^2_{sj-l_n}}{m^2_{sj}} \tag{27}$$

where m_{sj} represents the invariant mass of the sub-jet associated with the lepton and m_{sj-l_n} represents the invariant mass of the same sub-jet with the n^{th} lepton subtracted out.

We now concentrate on the distributions of the aforementioned variables for two and three inclusive fatjet searches, where the signal and dominant SM background contributions are shown together to characterize the differences between their distributions. The normalized distributions are shown with events that have passed the following selection cuts:

$$P_T^{\text{lepton}} > 25\ \text{GeV}; \quad P_T^{\text{fatjet}} > 200\ \text{GeV}; \quad |\eta^{\text{fatjet}}| < 4. \tag{28}$$

In Figs. 4 and 5, we show the relevant distributions of the selected kinematic variables in the *two-fatjet inclusive* search for BP2. In the *top-panel* of Fig. 4, we have shown the P_T distribution of the leading and subleading fatjet where a pre-selection cut of $P_T > 200$ GeV (before grooming for two leading fatjets) is in place. The distribution for the signal events peak at higher values of P_T because of the large mass gap between the decay products and their mother particles. In contrast, the background events, say from the $t\bar{t}$ production where the jets come from the decay of SM W bosons (including the b-jet), have relatively softer P_T beyond the pre-selection cut. Note that for the top quarks to be highly boosted, they would have to be produced at large $\sqrt{\hat{s}}$ which would lead to a smaller cross section for the $t\bar{t}$ production. The QCD multijet background also falls off rapidly for large P_T. The *middle-panel* of Fig. 4 shows the jet mass (m_j) distributions of the two leading fatjets, while the *bottom-panel* shows the distribution of the invariant mass of the two leading fatjets. For the signal events, one finds that the distributions in both m_{j_1} and m_{j_2} show two peaks that appear at the mass values of the heavy neutrinos (especially ν_4 and ν_5), whose highly boosted decay products correspond to the reconstructed fatjets. The jet-mass variable therefore helps us reconstruct the intermediate particles for the signal, which in turn also helps us to reject a large part of the SM background, where no such peak is observed at large values of m_j's.

Figure 5 highlights the relevance of the substructure variables used in our analysis. The *top-panel* shows the event distribution of the signal and background as a function of P_T of the sub-jets inclusive of the leading and sub-leading charged lepton. As expected, the signal fatjets which carry much larger P_T than the fatjets in the SM background events also give larger P_T sub-jets within them, leading to the sub-jets also getting a hard P_T distribution compared to the background. The *middle-* and *bottom-panels* of Fig. 5 display the event distributions as a function of LSF and LMD variables, respectively. The LSF variables are found to sharply peak around 1 for the signal and the $t\bar{t}$ (leptonic and semileptonic) background. This happens when the lepton is boosted enough and becomes one of the hardest constituents in the fatjet. As the signal and $t\bar{t}$ (leptonic and semileptonic) channels are most likely to give a fatjet with a non-isolated charged lepton within, these modes are the only ones that show the peak behavior around 1. Note that the peak has vanished in the distribution of LSF_2 for the $t\bar{t}$ (semileptonic), as only one top decays in the leptonic channel. It is therefore less likely to give a second charged lepton inclusive fatjet. In addition, the charge leptons do not suffer from soft radiations into the sub-jets, and we can reconstruct the energy of the lepton by finding the sub-jet. In the case of the QCD-multijet and $t\bar{t}$ hadronic background, most of the events correspond to some jet faking a lepton. As they shower, they are surrounded by soft collinear radiation, and when we get the sub-jet associated with it, additional soft radiation gets added up. Thus the LSF in most of the cases has a smaller value than one. The

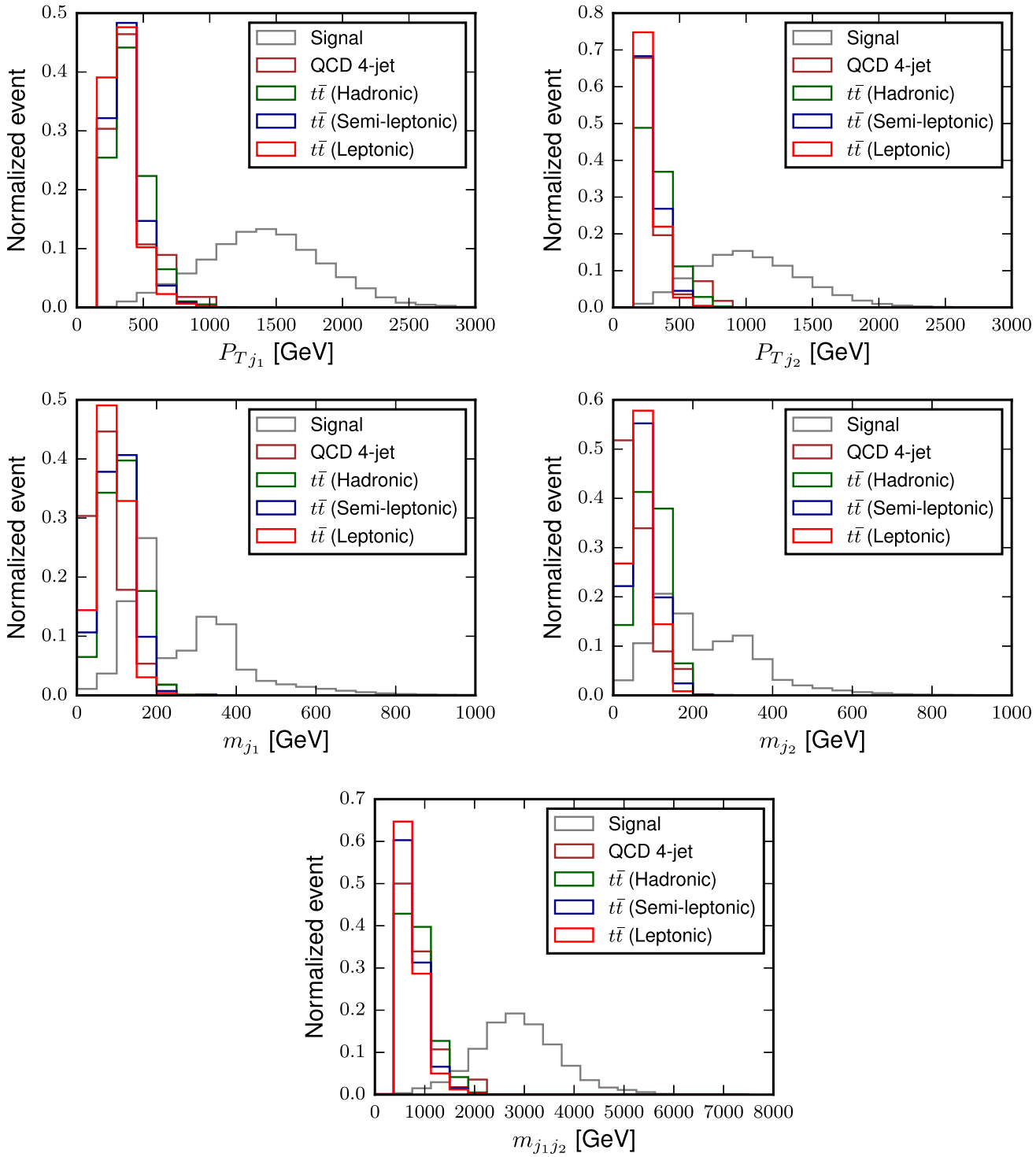

Fig. 4 Normalized distributions of the signal and different SM backgrounds as a function of the transverse momentum (P_T) of the two leading fatjets (top-panel), the mass (m_j) of two leading fatjets (middle-panel), and invariant mass ($m_{j_1 j_2}$) of the two leading fatjets (bottom-panel) in the *two-fatjet inclusive* searches for BP2

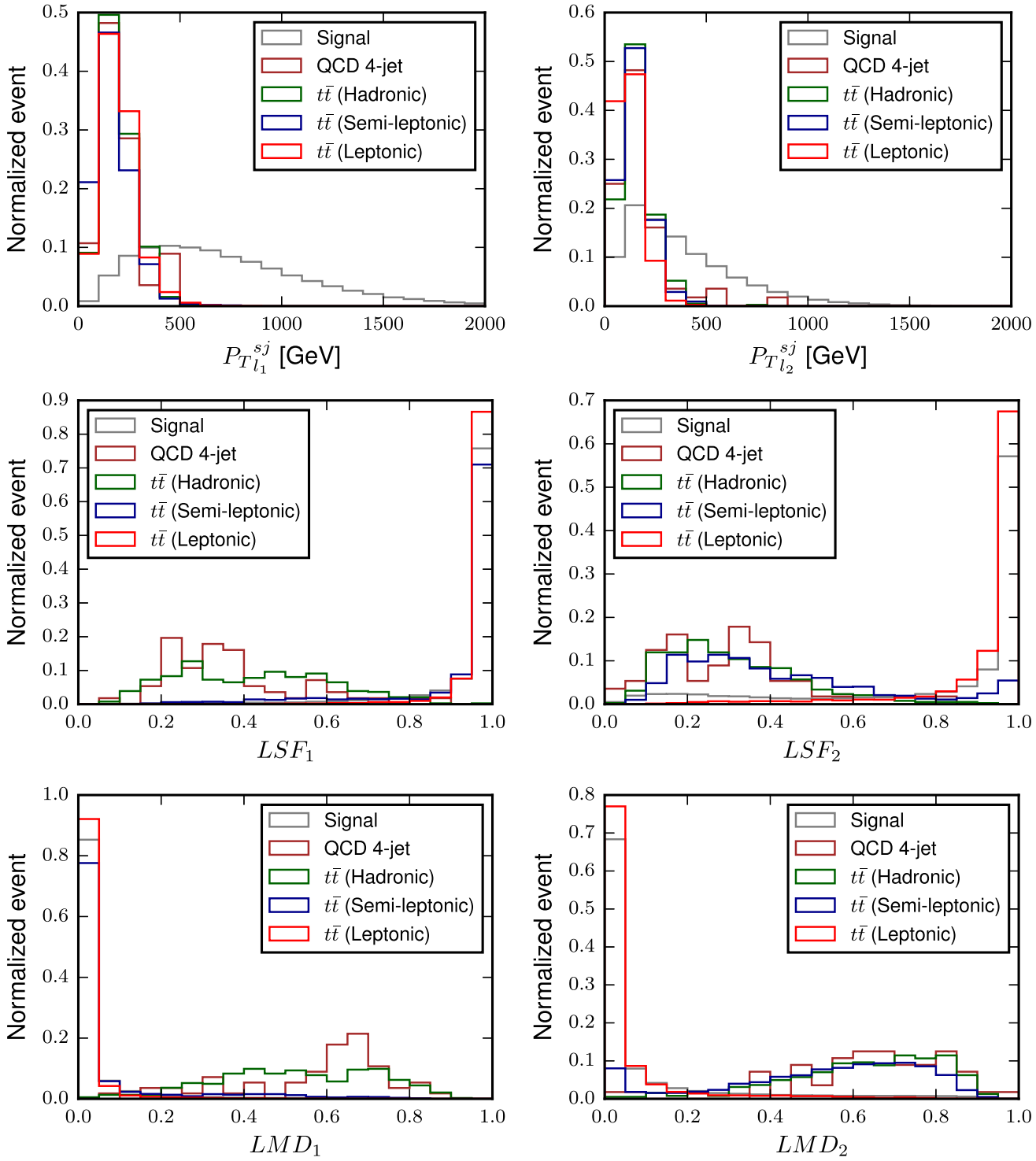

Fig. 5 Normalized distributions of the signal and different SM backgrounds as a function of the transverse momentum of the leptonic sub-jet ($P_{T_l^{sj}}$) of the fatjets (top-panel), the lepton sub-jet fraction variable involving the leading (LSF_1) and sub-leading (LSF_2) charged lepton (middle-panel) and the lepton mass drop variable with the leading (LMD_1) and sub-leading (LMD_2) charged lepton subtracted out (bottom-panel) in the *two-fatjet inclusive* searches for BP2

lepton mass drop (LMD) variable displays similar properties for the participating leptons within the fatjet. As the numerator in LMD, given by Eq. (27) represents the invariant mass of the sub-jet with the charged lepton removed, it peaks near zero due to the unlikeliness of the absence of charged leptons in the $t\bar{t}$ (leptonic and semileptonic) and the signal events, whereas it gives non-zero values for QCD-multijet and $t\bar{t}$ hadronic background where the leptons are conspicuous by their absence.

The kinematic distributions in the same variables for the three-fatjet inclusive analysis, show very similar features and are collected in Appendix B as Figs. 6, 7 and 8 for reference. The four-fatjet inclusive search is expected to be almost without any SM background and we focus only on the event rates for this final state.

4.3 Results

We now use the kinematic variables discussed in the previous section and exploit their characteristic distributions for signal and background to define the event selection cuts we use to analyze the three different fatjet signals. We have used a pre-selection criterion for signal and background in all our subsequent analyses given by:

Pre-selection criteria: For the pre-selection of events, we demand at least two charged leptons (e, μ) with $P_T > 25$ GeV at the event generation level along with two fat jets with radius $R = 0.8$ and minimum $P_T > 200$ GeV which must lie within the rapidity gap of $|\eta| < 4$ for the ungroomed jet. As pointed out earlier, the strong pre-selection cut on the fatjet P_T helps suppress the background events, dominantly coming from the QCD multijet processes. As the QCD background has a huge cross section, it is quite challenging to generate uniformly populated events in our simulations. The pre-selection cuts at the generation level allow us to lower the large QCD cross section to manageable numbers for event generation. We have checked that the signal events are not affected much by the pre-selection cuts used in our analysis.

Two-fatjet inclusive searches: The two-fatjet signal gives the largest cross section among all the fatjet signals. The signal and background distributions shown in Figs. 4 and 5 are used to define the event selection criterion to help achieve a good signal significance. We classify the kinematic selections for the signal and background events into two categories, which we call **Cut-A** and **Cut-B**.

Cut-A:

i. The leading groomed fatjet is required to have $P_{T\,j_1} > 750$ GeV, while the sub-leading groomed fatjet should have $P_{T\,j_2} > 500$ GeV.
ii. The jet mass of both the leading and sub-leading groomed fatjet should have a minimum value of $m_{j_i} > 125$ GeV ($i = 1, 2$) while their invariant mass must satisfy $m_{j_1 j_2} > 1.5$ TeV.
iii. The sub-jets associated with the leading charged lepton must have $P_T{}^{sj}_{l_1} > 400$ GeV and sub-jets associated with the sub-leading charged lepton are required to have $P_T{}^{sj}_{l_2} > 250$ GeV.
iv. The variables LSF_1 and LSF_2 need to be > 0.9, while LMD_1 and LMD_2 has an upper limit satisfying < 0.05 after applying the grooming method.

Cut-B:

i. The leading groomed fatjet is required to have $P_{T\,j_1} > 750$ GeV, while the sub-leading groomed fatjet must have $P_{T\,j_2} > 500$ GeV.
ii. The minimum value for the variables LSF_1 and LSF_2 is > 0.9, while the maximum value for LMD_1 and LMD_2 is < 0.05 after applying grooming method.

A summary of all cuts mentioned here is also described in Table 5.

Note that the main difference between **Cut-A** and **Cut-B** is simply on the way the lepton inclusive fatjets are treated, along with how we utilize the jet mass in the analysis which carries a bias of the mass of the new exotics. We list the number of signal and background events expected with an integrated luminosity of $\mathscr{L} = 3000$ fb^{-1} for `BP1` in Table 6. We also list the cross sections for different signal sub-processes contributing to the two-fatjet inclusive search. The events with **Cut-A** and **Cut-B** are shown in Tables 13 and 14 for `BP2`, and `BP3` in Appendix C.

As the signal events are peaked at very high P_T (Fig. 4) the strong cut on their P_T removes all of the background events coming from the QCD multijet and the hadronic decay of the $t\bar{t}$ production. In addition, the choice on the jet mass, invariant mass of the di-fatjet system and the additional cuts on the jet substructure variables are used to exploit the presence of the highly boosted charged lepton and are helpful to remove the background events coming from the leptonic decay modes of the $t\bar{t}$ production (Fig. 5). For all the `BP`s, we conclude that it is possible to remove the SM background with moderate efficiency using the pre-selection cuts, which is significantly improved after using **Cut-A** and **Cut-B**. We also note that **Cut-A** is a much stronger selection criterion compared to **Cut-B** as it requires an additional condition on the jet mass and invariant mass of the fatjet pairs, which reduces the signal events too. Therefore, **Cut-A** will yield better significance where the production cross section of the signal is relatively large, while **Cut-B** will perform better where the signal cross section is small, and we do not want a signification reduction in the event rates for the signal.

Table 5 Cut summary for two-fatjet inclusive searches

Cut summary		
Pre-selection cut	Cut-A	Cut-B
• Number of leptons, $N_l \geq 2$ with $P_T > 25$ GeV • Two fatjets with radius $R = 0.8$ • Rapidity gap of two ungroomed fatjet, $\|\Delta\eta\| < 4$	• $P_{T\,j_1} > 750$ GeV, $P_{T\,j_2} > 500$ GeV • $LSF_1 > 0.9$, $LSF_2 > 0.9$ • $LMD_1 < 0.05$, $LMD_2 < 0.05$ • $P_T{}^{sj}_{l_1} > 400$ GeV, $P_T{}^{sj}_{l_2} > 250$ GeV • $m_{j_i} > 125$ GeV $(i = 1, 2)$; $m_{j_1 j_2} > 1.5$ TeV	• $P_{T\,j_1} > 750$ GeV, $P_{T\,j_2} > 500$ GeV • $LSF_1 > 0.9$, $LSF_2 > 0.9$ • $LMD_1 < 0.05$, $LMD_2 < 0.05$

Table 6 Signal and background events surviving after applying the pre-selection criteria as well as selection cuts at LHC with center-of-mass energy, $\sqrt{s} = 14$ TeV and $\mathscr{L} = 3000$ fb^{-1} in the inclusive two-fatjet analysis for BP1

Data sets	Cross section (pb)		Number of events	
	Parton-level	Pre-selection cut	**Cut-A**	**Cut-B**
$W_R \to e_6\nu_5, e_6 \to \mu jj$	0.021×10^{-6}	3	1	2
$W_R \to e_6\nu_5, e_6 \to \nu_5 jj$	0.400×10^{-3}	269	77	150
$W_R \to E_4\nu_4$	0.485×10^{-3}	660	51	225
$Z_R \to (\nu_4\nu_4)/(\nu_5\nu_5)$	0.110×10^{-3}	189	40	93
$Z_R \to E_4\bar{E}_4$	0.012×10^{-3}	8	1	2
Total signal (s)		1129	170	472
QCD 4-jet	90387.504	1.52×10^7	0	0
$t\bar{t}$ (hadronic)	229.603	2.65×10^5	0	0
$t\bar{t}$ (semi-leptonic)	178.569	7.94×10^5	0	0
$t\bar{t}$ (leptonic)	34.854	7.43×10^5	105	1.568×10^3
Total background (b)		1.7×10^7	105	1.568×10^3

We calculate the signal significance [74] using the formula

$$\mathscr{S} = \sqrt{2\left[(s+b)\log\left(1+\frac{s}{b}\right) - s\right]}, \tag{29}$$

where s and b stand for the total number of signal and background events surviving after cuts and $\mathscr{L}$ is the integrated luminosity. The signal significances for all the BPs in the inclusive two-fatjet final state are summarized in Table 7, with integrated luminosities of 3000 fb^{-1}, 600 fb^{-1} and 300 fb^{-1} at the LHC with a center-of-mass energy $\sqrt{s} = 14$ TeV. For BP1, we are able to achieve a significance of more than 5σ at $\mathscr{L} = 600$ fb^{-1}, while for BP2, which represents a point with a heavier W_R, we need 3000 fb^{-1} luminosity to achieve 5σ significance. This is due to the large mass of W_R and Z_R in BP2 compared to BP1, which reduces the production cross section of the contributing sub-processes for BP2, although the cut efficiency for the signal events is better in the case of BP2. In the case of BP3, the signal significance is better compared to BP2 because of the larger production cross section and higher boost for the heavy leptons. For BP3, an integrated luminosity of 600 fb^{-1} is required for a 5σ discovery. We note that **Cut-A** and **Cut-B** provide roughly the same amount of significance for BP1. While for BP2 and BP3, **Cut-A** gives better significance as the jet mass and P_T of sub-jets play an important role in reducing the background further.

Table 7 Signal significance for the two-fatjet signals for different cuts at the LHC with a center-of-mass energy $\sqrt{s} = 14$ TeV with $\mathscr{L} = 3000$ fb^{-1}, $\mathscr{L} = 600$ fb^{-1} and $\mathscr{L} = 300$ fb^{-1}

After applying cut	3000 fb^{-1}	600 fb^{-1}	300 fb^{-1}
Cut-A (BP1)	13.77 σ	6.16 σ	4.35 σ
Cut-B (BP1)	11.39 σ	5.09 σ	3.60 σ
Cut-A (BP2)	7.36 σ	3.29 σ	2.33 σ
Cut-B (BP2)	5.24 σ	2.34 σ	1.66 σ
Cut-A (BP3)	11.11 σ	4.97σ	3.51 σ
Cut-B (BP3)	7.64 σ	3.42 σ	2.42 σ

Three-fatjet inclusive searches: We have already discussed the major signal contribution to three-fatjet inclusive searches for our scenario in Sect. 4.1.1. The distributions of various variables are also shown in Figs. 7 and 8. To analyze the three-fatjet final state events, we consider three different sets of kinematic selections (**Cut-A**, **Cut-B** and **Cut-C**). A sum-

Table 8 Cut summary for three-fatjet inclusive searches

Cut summary			
Pre-selection cut	Cut-A	Cut-B	Cut-C
• $N_l \geq 2$ with $P_T > 25$ GeV	• $P_{T\,j_1(j_2)} > 500(300)$ GeV	• $P_{T\,j_1(j_2)} > 750(500)$ GeV	• $P_{T\,j_1(j_2)} > 750(500)$ GeV
• Two fatjets with radius $R = 0.8$.	• $m_{j_i} > 150$ GeV ($i = 1, 2$), $m_{j_3} > 100$ GeV, $m_{j_1 j_2} > 800$ GeV	• $LSF_1 > 0.9$, $LSF_2 > 0.9$ • $LMD_1 < 0.05$, $LMD_2 < 0.05$	• $m_{j_i} > 150$ GeV ($i = 1, 2$), $m_{j_3} > 100$ GeV, $m_{j_1 j_2} > 1000$ GeV
• $\lvert\Delta\eta\rvert < 4$ of two ungroomed fatjet	• $P_T{}^{sj}_{l_1} > 100$ GeV		• $P_T{}^{sj}_{l_1} > 100$ GeV.

mary of all cuts mentioned below is also summarized in Table 8.

Cut-A:

i. The leading groomed fatjet is required to have $P_{T\,j_1} > 500$ GeV, while the sub-leading groomed fatjet should have $P_{T\,j_2} > 300$ GeV.
ii. The jet mass of both the leading and sub-leading groomed fatjet should have a minimum value of $m_{j_i} > 150$ GeV ($i = 1, 2$), while their invariant mass must satisfy $m_{j_1 j_2} > 800$ GeV. Additionally, the next-to-sub-leading groomed fatjet has jet mass of $m_{j_3} > 100$ GeV.
iii. The sub-jets associated with leading charged lepton must have $P_T{}^{sj}_{l_1} > 100$ GeV.

Cut-B:

i. The leading groomed fatjet is required to have $P_{T\,j_1} > 750$ GeV, while the groomed sub-leading fatjet should have $P_{T\,j_2} > 500$ GeV.
ii. The variables LSF_1 and LSF_2 have a minimum value of 0.9, while LMD_1 and LMD_2 are bounded from above by < 0.05 after applying grooming techniques.

Cut-C:

i. The leading groomed fatjet is required to have $P_{T\,j_1} > 750$ GeV, while the sub-leading groomed fatjet should have $P_{T\,j_2} > 500$ GeV.
ii. The jet mass of both the leading and sub-leading groomed fatjet should have a minimum value of $m_{j_i} > 150$ GeV ($i = 1, 2$), while their invariant mass must satisfy $m_{j_1 j_2} > 1000$ GeV. Additionally, the next-to-sub-leading groomed fatjet has jet mass of $m_{j_3} > 100$ GeV.
iii. The sub-jets associated with leading charged lepton must have $P_T{}^{sj}_{l_1} > 100$ GeV.

Note that the role of the cuts exploiting the P_T, jet mass, invariant mass of fatjet pairs, and the substructure variables, LSF and LMD remain very similar to the two-fatjet analysis, albeit with differences in the threshold choices for the event selection. The effect of the three sets of cuts on our signal and SM background is tabulated in Tables 15, 16, and 17 in Appendix C for BP1, BP2, and BP3, respectively. Here, **Cut-C** represents the strongest selection criteria for the events as it includes the additional requirements on the jet mass and a stronger cut on the di-fatjet invariant mass. We note that **Cut-B** which is the only set that includes the cut on the leptonic sub-jet variables, is useful in suppressing the the SM background most and also retains the maximum signal events. This is in agreement with our earlier observation in the two-fatjet analysis where we found that the jet-mass and invariant mass selections also suppress the signal events considerably. The signal significances for all the BPs are shown in Table 9 for $\mathscr{L} = 3000$ fb^{-1}, $\mathscr{L} = 600$ fb^{-1}, and 300 fb^{-1}. We find that **Cut-B** that includes the LSF and LMD substructure variables, gives the best signal significance as it retains the maximum signal events for all the BPs. **Cut-A** and **Cut-C** give similar but lower significance. In the three-fatjet inclusive analysis, we require $\mathscr{L} = 600$ fb^{-1} for BP1 and $\mathscr{L} \approxeq 3000$ fb^{-1} for BP2 and BP3 to achieve 5σ discovery.

Table 9 Signal significance for the three-fatjet signals for different cuts at the LHC with a center-of-mass energy $\sqrt{s} = 14$ TeV with $\mathscr{L} = 3000$ fb^{-1}, $\mathscr{L} = 600$ fb^{-1} and $\mathscr{L} = 300$ fb^{-1}

After applying cut	3000 fb^{-1}	600 fb^{-1}	300 fb^{-1}
Cut-A (BP1)	3.13 σ	1.40 σ	0.99 σ
Cut-B (BP1)	15.35 σ	6.87 σ	4.85 σ
Cut-C (BP1)	3.00 σ	1.34 σ	0.95 σ
Cut-A (BP2)	1.58 σ	0.71 σ	0.50 σ
Cut-B (BP2)	7.92 σ	3.54 σ	2.5 σ
Cut-C (BP2)	1.54 σ	0.69 σ	0.49 σ
Cut-A (BP3)	2.08 σ	0.93 σ	0.66 σ
Cut-B (BP3)	8.31 σ	3.72 σ	2.63 σ
Cut-C (BP3)	2.04 σ	0.91 σ	0.65 σ

Four-fatjet inclusive searches: An interesting and more exotic signal for the model would be in the form of four fatjets. However, for such a final state, one can expect a very low signal cross section for our benchmark choices as only the $p\,p \to Z_R \to E_4 \bar{E}_4$ process contributes and is suppressed due to the large Z_R mass (already bounded from below due

Table 10 Cut summary for four-fatjet inclusive searches

Cut summary	
Pre-selection cut	**Cut-A**
• $N_l \geq 2$ with $P_T > 25$ GeV	• $P_{T\,j_1} > 500$ GeV, $P_{T\,j_2} > 300$ GeV
• Two fatjets with radius $R = 0.8$	• $m_{j_i} > 150$ GeV $(i = 1, 2)$, $m_{j_2} > 120$ GeV $(i = 1, 2)$
	• $m_{j_1 j_2} > 800$ GeV, $m_{j_1 j_2 j_3 j_4} > 1000$ GeV
• $\lvert\Delta\eta\rvert < 4$ of two ungroomed fatjet	• $P_{T\,l_1}^{sj} > 200$ GeV.

Table 11 Signal significance of the four-fatjet signals at the LHC with a center-of-mass energy $\sqrt{s} = 14$ TeV with $\mathscr{L} = 3000$ fb^{-1} and $\mathscr{L} = 600$ fb^{-1}

After applying cut	$\mathscr{L} = 3000$ fb^{-1}	$\mathscr{L} = 600$ fb^{-1}
Cut-A (BP1)	0.30 σ	0.13 σ
Cut-A (BP2)	0.11 σ	0.05 σ
Cut-A (BP3)	0.16 σ	0.07 σ

to the W_R mass limits in an LRSM framework). A part of the parameter space can be tuned to generate a conducive set of masses to improve some decay branching fractions, but we are still constrained by the luminosity reach of the LHC. The SM background is expected to be quite negligible for such a final state and this signal may prove useful to consider at more high-energy machines such as the future 100 TeV hadron collider [75]. As the LRSM gauge boson masses are excluded to be heavier and go beyond the reach of the LHC, the future hadron collider with $\sqrt{s} = 100$ TeV will be able to produce them easily and will give significantly large cross sections [76]. The large production rates will help study the four-fatjet signal very easily. For the sake of comparison, we go ahead and analyze our four-fatjet signal for the previously considered benchmark points to show what sensitivity could be expected at the LHC with a center-of-mass energy $\sqrt{s} =$ 14 TeV.

Placing similar pre-selection criteria as in the previous cases, we choose a single set of cuts to show our result:

Cut-A:

i. The P_T of leading fatjet, $P_{T\,j_1} > 500.0$ GeV and subleading fatjet, $P_{T\,j_2} > 300.0$ GeV.
ii. Jet mass of leading jet, $m_{j_1} > 150.0$ GeV and subleading jet, $m_{j_2} > 120.0$ GeV while invariant mass of leading and subleading jet, $m_{j_1 j_2} > 800.0$ GeV. Additionally, the invariant mass of all four fatjets, $m_{j_1 j_2 j_3 j_4} > 1000.0$ GeV.
iii. The P_T of sub jets associated with leading charged lepton satisfies $P_{T\,l_1}^{sj} > 200.0$ GeV.

We summarize our cuts for four-fatjet inclusive searches in Table 10.

As expected, we find that the four-fatjet analysis is not feasible with the available cross section for the signal and, therefore, will not be accessible at the LHC, even with $\mathscr{L} =$ 3000 fb^{-1} as shown in Table 11. This significance is further diminished if the LSF and LMD variables are invoked in our analysis.

5 Conclusion

In this work, we perform a collider study to look for fatjets originating from boosted particles that come from the decay of heavy resonances in a left-right symmetric extension of the SM. The model contains heavy leptons, heavy quarks, and heavy neutrinos, which play a fundamental role in achieving a universal seesaw mechanism for the generation of all the SM fermion masses. The fatjets, which include non-isolated leptons, originate from heavy neutrinos (few 100 GeV) that decay from a heavier (few TeV) right-handed gauge boson. We employ substructure-based variables LSF and LMD, together with hard kinematic cuts, to search for fatjets with associated charged leptons, to reduce SM background while keeping enough statistics for the signals.

We analyze a multi-fatjet signal topology that would be typical in the model when the heavy fermionic states are produced and finally decay to SM particles. We have focused mainly on two-fatjet and three-fatjet final state searches while commenting on the possibility of a four-fatjet scenario with very limited signal sensitivity for our parameter choices. A critical aspect of the analysis included the presence of a charged lepton in the fatjets, helping us identify the signal over the SM background by employing the variables LSF and LMD.

In the two-fatjet final state, both jets include a charged lepton, while for three-fatjet, two of them include a charged lepton. We find that the two-fatjet signals, which also include leptons, can be discovered at the LHC with a moderate luminosity of $\mathscr{L} \simeq 600$ fb^{-1} for $m_E \simeq 1$ TeV, $m_{W_R} = 4.5$ TeV (BP1) and $m_E \simeq 0.72$ TeV, $m_{W_R} = 5$ TeV (BP3), while the signal can be discovered with $\mathscr{L} \simeq 3000$ fb^{-1} for $m_E \simeq 1$ TeV, $m_{W_R} \simeq 5$ TeV (BP2), as shown in Table 7. On the other hand, a three-fatjet signal can be discovered with $\mathscr{L} \simeq 600$ fb^{-1} (see Table 9) for $m_{W_R} = 4.5$ TeV (BP1). In the case of

$m_{W_R} = 5$ TeV (BP2 and BP3), we require $\mathscr{L} \simeq 3000$ fb^{-1} for a 5σ discovery.

We finally conclude by noting that although these signals of fatjet can have origins from an altogether different underlying theoretical framework compared to left-right symmetry or a seesaw framework, their observation will be still crucial in the search of new physics at LHC and will provide hints on the presence of new heavy states beyond the SM.

Acknowledgements The authors would like to acknowledge support from the Department of Atomic Energy, Government of India, for the Regional Centre for Accelerator-based Particle Physics (RECAPP), Harish Chandra Research Institute.

Data Availability Statement This manuscript has no associated data or the data will not be deposited. [Authors' comment: The authors do not have any extra comments regarding data availability statement.]

Funded by SCOAP^3.

Appendix A: Decay branching ratios in BP2 and BP3

We present the relevant branching ratios (BR) for the decay modes of the heavy $SU(2)_R$ gauge bosons W_R and Z_R, the heavy leptons E_i, and three heavy neutrinos ν_i (with $i = 4, 5, 6$) for BP2 and BP3 in Table 12. The BRs of the particles in BP1 and BP2 remain roughly the same due to the identical mass of the heavy charged leptons. In contrast, there are subtle changes on the BRs in BP3 due to the smaller mass of the heavy charged leptons. Among the relevant BRs, the di-jet BR of the heavy gauge bosons are reduced by approximately 2–3%, BR($W_R \to e\nu_4$) is reduced by roughly 2%, while BR($W_R \to E_4\nu_4$) is increased by 2%. The other BRs in BP3 are roughly the same as those in BP1.

Table 12 Decay branching ratios for W_R and Z_R, heavy charged leptons E_i, and the lightest three heavy neutrinos ν_i, $(i = 4, 5, 6)$ for BP2 and BP3

Decay	Branching BP2 (%)	BP3 (%)
$W_R^+ \to jj$	65.0	63.0
$W_R^+ \to t\bar{b}$	10.0	9.80
$W_R^+ \to e^+\nu_4$	4.96	3.20
$W_R^+ \to \mu^+\nu_5$	1.56	0.700
$W_R^+ \to \tau^+\nu_6$	2.40	1.40
$W_R^+ \to E_4^+\nu_4$	5.20	7.00
$W_R^+ \to E_5^+\nu_6$	5.48	7.21
$W_R^+ \to E_6^+\nu_5$	5.30	7.31
$Z_R \to jj$	46.9	45.9
$Z_R \to \nu_4\nu_4$	7.09	6.94
$Z_R \to \nu_5\nu_5$	6.52	6.38
$Z_R \to E_4\bar{E}_4$	2.27	2.40
$Z_R \to E_5\bar{E}_5$	1.41	2.28
$E_4 \to \nu_4 jj$	70.7	70.4
$E_5 \to \nu_6 jj$	5.88	0.712
$E_6 \to \nu_5 jj$	73.7	77.9
$E_6 \to \mu jj$	3.66	2.18
$\nu_4 \to e^\pm jj$	100	100
$\nu_5 \to \mu^\pm jj$	94.5	95.0
$\nu_6 \to \tau^\pm jj$	87.4	88.6

Appendix B: Kinematical distributions for fatjets in three-fatjet searches

The normalized distributions for the kinematic variables, such as the P_T of the fatjets, P_T of the two leading lepton subjects, invariant mass of the fatjets, the LSF and LMD in the case of three-fatjet search are shown in Figs. 6, 7 and 8.

The distributions are similar to the distributions of two-fatjet searches as described above in the main texts. In particular, the invariant mass constructed out of the three fatjets shown in Fig. 6, is identified as a good observable to separate signals from backgrounds.

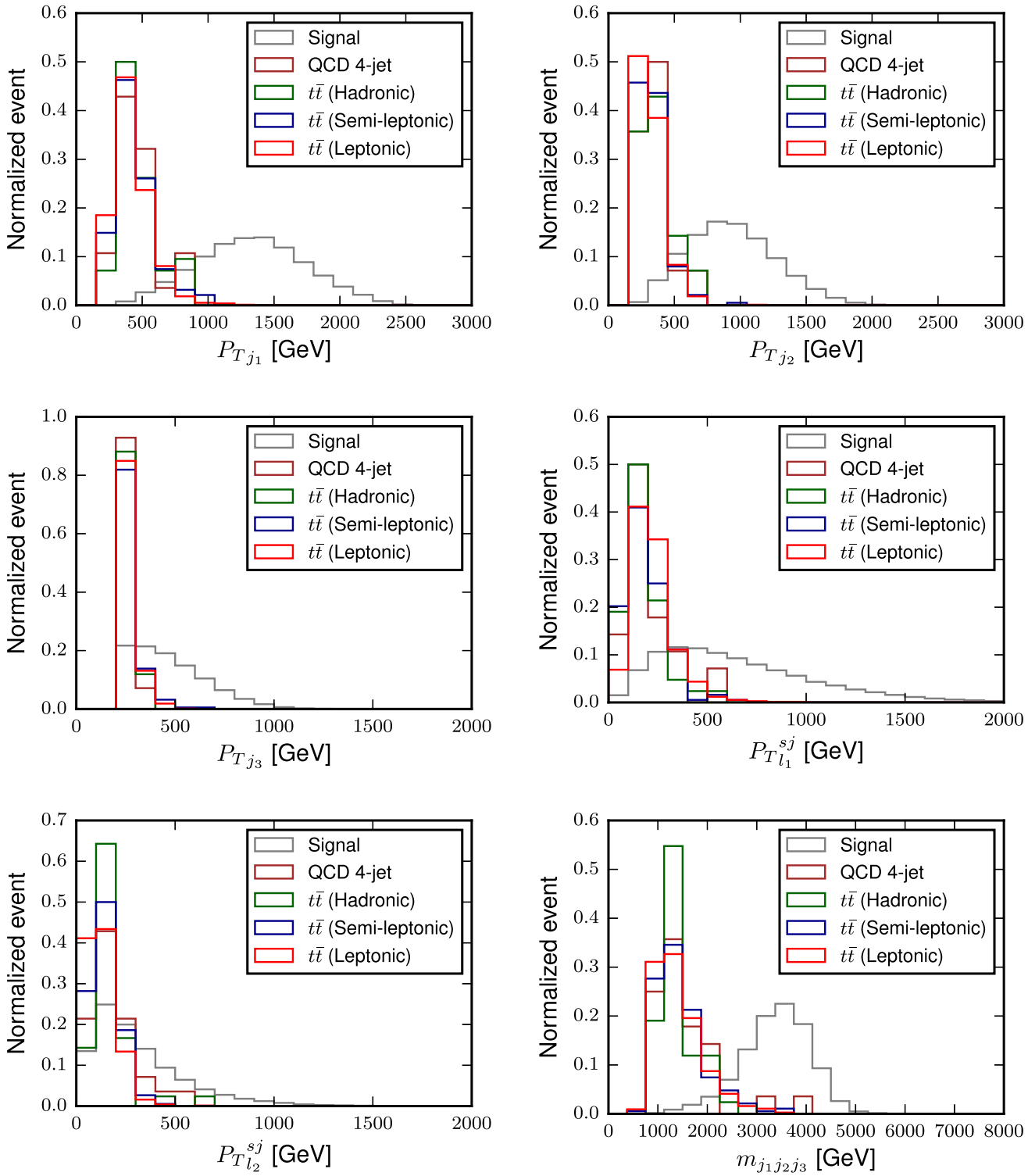

Fig. 6 Normalized distributions of the signal and different SM backgrounds as a function of the transverse momentum (P_T) of the three leading fatjets, the transverse momentum of the leptonic sub-jets ($P_{T_l^{sj}}$) in the fatjets and invariant mass ($m_{j_1\,j_2\,j_3}$) of the three leading fatjets in the *three-fatjet inclusive* searches for BP2

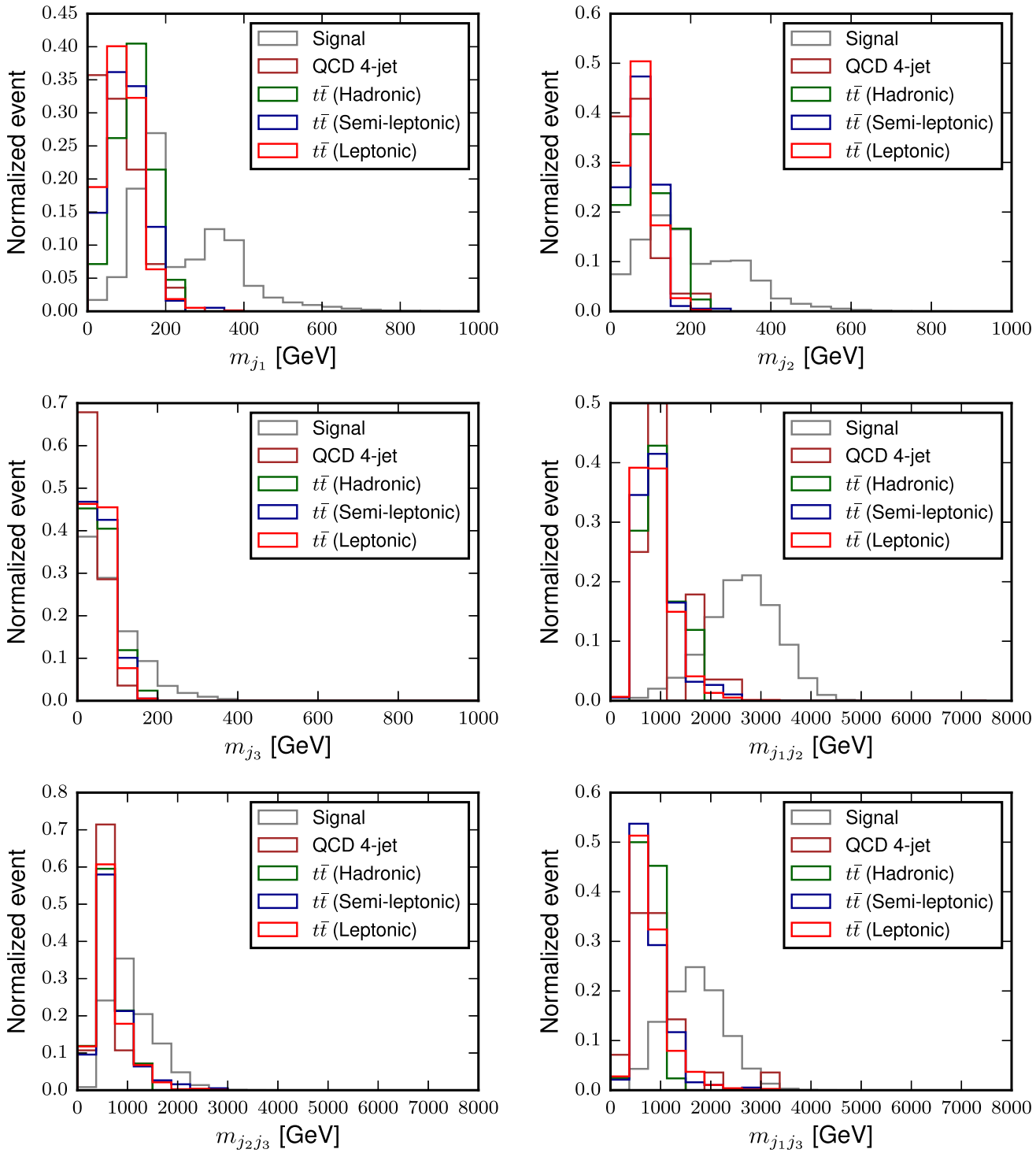

Fig. 7 Normalized distributions of the signal and different SM backgrounds as a function of the mass (m_{j_i}) of three leading fatjets and the invariant mass ($m_{j_a\, j_b}$, a,b=1,2,3) in the *three-fatjet inclusive* searches for BP2

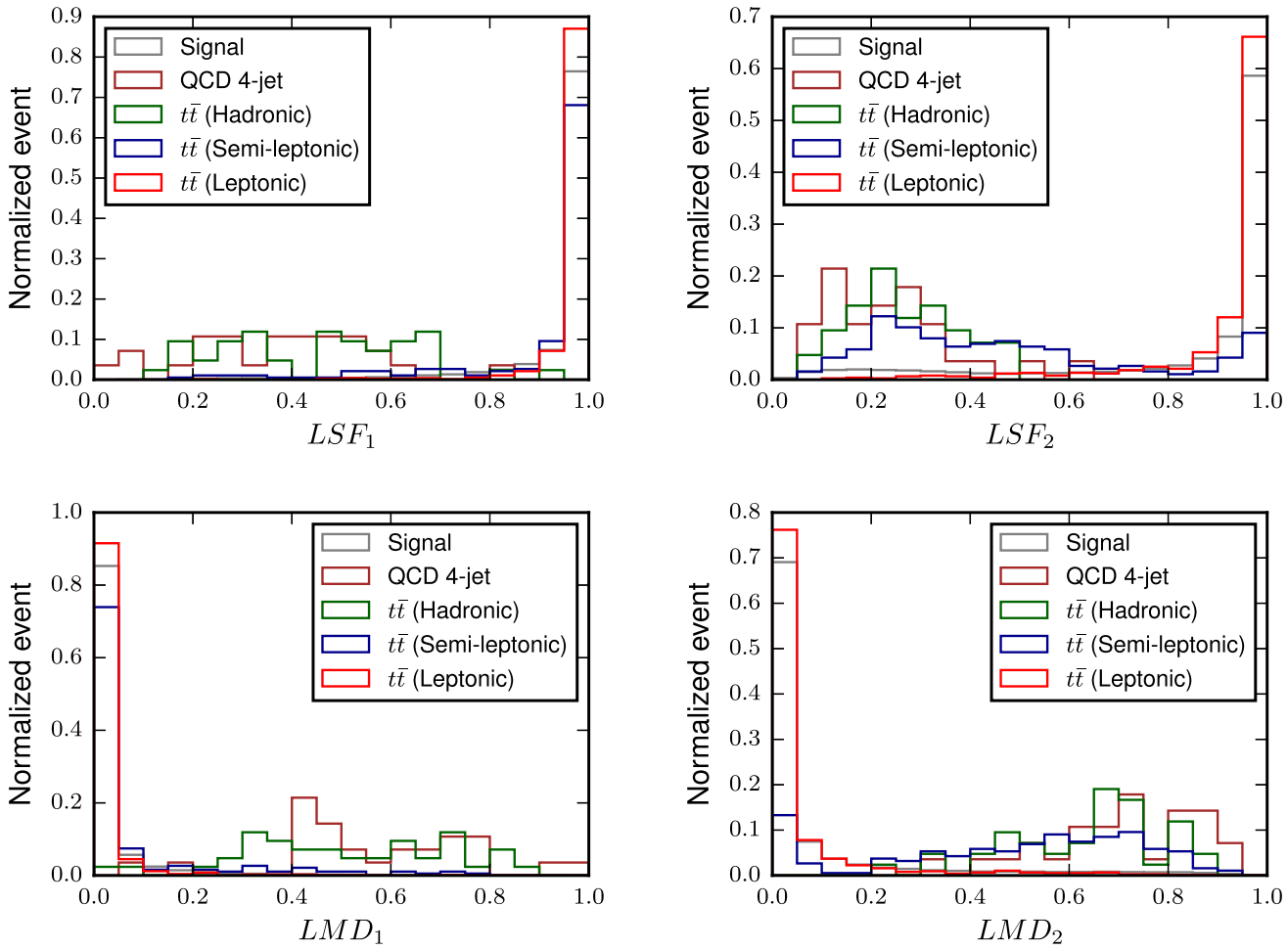

Fig. 8 Normalized distributions of the signal and different SM backgrounds as a function of LSF and LMD in the *three-fatjet inclusive* searches for BP2

Appendix C: Signal and background events surviving after different cuts for different benchmark points

We list the number of signal events and background events after applying the pre-selection cuts and different selection cuts in Tables 13 and 14 for two-fatjet searches in BP2 and BP3, respectively. For three-fatjet searches, the signal and background events after different cuts are listed in Tables 15, 16, and 17 for BP1, BP2, and BP3, respectively.

Table 13 Signal and background events surviving after applying the pre-selection criteria as well as selection cuts at $\sqrt{s} = 14$ TeV and $\mathscr{L} = 3000$ fb^{-1} for two-fatjet searches in BP2. The individual contributions of SM subprocesses to the background are as shown in Table 6

Data sets	Cross section (pb)		Number of events	
	Parton-level	Pre-selection cut	**Cut-A**	**Cut-B**
$W_R \to E_6\nu_5, E_6 \to \mu jj$	0.009424×10^{-3}	4	1	1
$W_R \to E_6\nu_5, E_6 \to \nu_5 jj$	0.18038×10^{-3}	146	46	83
$W_R \to E_4\nu_4$	0.19974×10^{-3}	286	22	93
$Z_R \to (\nu_4\nu_4)/(\nu_5\nu_5)$	0.04861×10^{-3}	75	15	34
$Z_R \to E_4\bar{E}_4$	0.004374×10^{-3}	4	0	1
Total Signal (s)		515	84	212
Total Background (b)		1.7×10^7	105	1.568×10^3

Table 14 Signal and background events surviving after applying the pre-selection criteria as well as selection cuts at $\sqrt{s} = 14$ TeV and $\mathscr{L} = 3000$ fb^{-1} for two-fatjet searches in BP3. The individual contributions of SM subprocesses to the background are as shown in Table 6

Data sets	Cross section (pb)		Number of events	
	Parton-level	Pre-selection cut	**Cut-A**	**Cut-B**
$W_R \to e_6\nu_5, e_6 \to \mu jj$	0.009×10^{-3}	2	1	1
$W_R \to e_6\nu_5, e_6 \to \nu_5 jj$	0.279×10^{-3}	271	83	152
$W_R \to E_4\nu_4$	0.295×10^{-3}	519	34	125
$Z_R \to (\nu_4\nu_4)/(\nu_5\nu_5)$	0.048×10^{-3}	73	14	33
$Z_R \to E_4\bar{E}_4$	0.006 fb	7	1	1
Total Signal (s)		872	133	312
Total Background (b)		1.7×10^7	105	1.568×10^3

Table 15 Signal and background events surviving after applying the pre-selection criteria as well as selection cuts at $\sqrt{s} = 14$ TeV and $\mathscr{L} = 3000$ fb^{-1} for three-fatjet searches in BP1

Data sets	Cross section (pb)		Number of events		
	Parton-level	Pre-selection cut	**Cut-A**	**Cut-B**	**Cut-C**
$W_R \to e_6\nu_5$	0.400×10^{-3}	378	51	88	49
$W_R \to E_4\nu_4$	0.485×10^{-3}	607	22	104	21
$Z_R \to E_4\bar{E}_4$	0.012×10^{-3}	11	1	1	1
Total Signal (s)		996	74	193	114
QCD 4-jet	90387.504	7.59×10^6	0	0	0
$t\bar{t}$ (Hadronic)	229.603	2.89×10^4	0	0	0
$t\bar{t}$ (Semi-leptonic)	178.569	1.01×10^5	536	0	536
$t\bar{t}$ (Leptonic)	34.854	7.9×10^4	0	105	0
Total Background (b)		7.8×10^6	536	105	536

Table 16 Signal and background events surviving after applying the pre-selection criteria as well as selection cuts at $\sqrt{s} = 14$ TeV and $\mathscr{L} = 3000$ fb^{-1} for three-fatjet searches in BP2. The individual contributions of SM subprocesses to the background are as shown in Table 15

Data sets	Cross section (pb)		Number of events		
	Parton-level	Pre-selection cut	**Cut-A**	**Cut-B**	**Cut-C**
$W_R \to E_4\nu_4$	0.199×10^{-3}	251	9	42	8
$W_R \to E_6\nu_5$	0.180×10^{-3}	207	28	49	28
$Z_R \to E_4\bar{E}_4$	0.004×10^{-3}	4	0	0	0
Total Signal (s)		462	37	91	36
Total Background (b)		7.8×10^6	536	105	536

Table 17 Signal and background events surviving after applying the pre-selection criteria as well as selection cuts at $\sqrt{s} = 14$ TeV and $\mathscr{L} = 3000$ fb^{-1} for three-fatjet searches in BP3. The individual contributions of SM subprocesses to the background are as shown in Table 15

Data sets	Cross section (pb)	Number of events			
	Parton-level	Pre-selection cut	**Cut-A**	**Cut-B**	**Cut-C**
$W_R \to e_6\nu_5$	0.279×10^{-3}	313	46	79	45
$W_R \to E_4\nu_4$	0.295×10^{-3}	162	3	17	3
$Z_R \to E_4\bar{E}_4$	0.006×10^{-3}	2	0	0	0
Total Signal (s)		477	49	96	48
Total Background (b)		7.8×10^6	536	105	536

References

1. SNO Collaboration, Q.R. Ahmad et al., Direct evidence for neutrino flavor transformation from neutral current interactions in the Sudbury Neutrino Observatory. Phys. Rev. Lett. **89**, 011301 (2002). https://doi.org/10.1103/PhysRevLett.89.011301. arXiv:nucl-ex/0204008
2. Super-Kamiokande Collaboration, Y. Fukuda et al., Evidence for oscillation of atmospheric neutrinos. Phys. Rev. Lett. **81**, 1562–1567 (1998). https://doi.org/10.1103/PhysRevLett.81.1562. arXiv:hep-ex/9807003
3. KamLAND Collaboration, K. Eguchi et al., First results from KamLAND: evidence for reactor anti-neutrino disappearance. Phys. Rev. Lett. **90**, 021802 (2003). https://doi.org/10.1103/PhysRevLett.90.021802. arXiv:hep-ex/0212021
4. I. Esteban, M.C. Gonzalez-Garcia, M. Maltoni, T. Schwetz, A. Zhou, The fate of hints: updated global analysis of three-flavor neutrino oscillations. JHEP **09**, 178 (2020). https://doi.org/10.1007/JHEP09(2020)178. arXiv:2007.14792 [hep-ph]
5. I. Esteban, M.C. Gonzalez-Garcia, M. Maltoni, T. Schwetz, A. Zhou, NuFIT 5.0: Three-neutrino fit based on data available in July 2020. http://www.nu-fit.org/?q=node/228
6. R.N. Mohapatra, J.C. Pati, A natural left-right symmetry. Phys. Rev. D **11**, 2558 (1975). https://doi.org/10.1103/PhysRevD.11.2558
7. R.N. Mohapatra, J.C. Pati, Left-Right gauge symmetry and an isoconjugate model of CP violation. Phys. Rev. D **11**, 566–571 (1975). https://doi.org/10.1103/PhysRevD.11.566
8. G. Senjanovic, R.N. Mohapatra, Exact left-right symmetry and spontaneous violation of parity. Phys. Rev. D **12**, 1502 (1975). https://doi.org/10.1103/PhysRevD.12.1502
9. G. Senjanovic, Spontaneous breakdown of parity in a class of gauge theories. Nucl. Phys. B **153**, 334–364 (1979). https://doi.org/10.1016/0550-3213(79)90604-7
10. P. Minkowski, $\mu \to e\gamma$ at a rate of one out of 10^9 muon decays? Phys. Lett. B **67**, 421–428 (1977). https://doi.org/10.1016/0370-2693(77)90435-X
11. O. Sawada, A. Sugamoto, eds., *Proceedings: Workshop on the Unified Theories and the Baryon Number in the Universe: Tsukuba, Japan, February 13-14, 1979*. Natl. Lab. High Energy Phys., Tsukuba, Japan, 1979. https://inspirehep.net/literature/19833
12. S.L. Glashow, The future of elementary particle physics. NATO Sci. Ser. B **61**, 687 (1980). https://doi.org/10.1007/978-1-4684-7197-7_15
13. R.N. Mohapatra, G. Senjanovic, Neutrino mass and spontaneous parity nonconservation. Phys. Rev. Lett. **44**, 912 (1980). https://doi.org/10.1103/PhysRevLett.44.912
14. V.A. Kuzmin, M.E. Shaposhnikov, Baryon asymmetry of the universe versus left-right symmetry. Phys. Lett. B **92**, 115 (1980). https://doi.org/10.1016/0370-2693(80)90317-2
15. V.A. Kuzmin, V.A. Rubakov, M.E. Shaposhnikov, On the anomalous electroweak Baryon number nonconservation in the early universe. Phys. Lett. B **155**, 36 (1985). https://doi.org/10.1016/0370-2693(85)91028-7
16. J.M. Frere, L. Houart, J.M. Moreno, J. Orloff, M. Tytgat, Generation of the baryon asymmetry of the universe within the left-right symmetric model. Phys. Lett. B **314**, 289–297 (1993). https://doi.org/10.1016/0370-2693(93)91238-I. arXiv:hep-ph/9301228
17. A.S. Abhishek, U.A. Yajnik, PeV scale left-right symmetry and baryon asymmetry of the Universe. Nucl. Phys. B **800**, 253–269 (2008). https://doi.org/10.1016/j.nuclphysb.2008.03.020
18. R.N. Mohapatra, G. Senjanovic, Natural suppression of strong p and t noninvariance. Phys. Lett. B **79**, 283–286 (1978). https://doi.org/10.1016/0370-2693(78)90243-5
19. K.S. Babu, R.N. Mohapatra, CP violation in seesaw models of quark masses. Phys. Rev. Lett. **62**, 1079 (1989). https://doi.org/10.1103/PhysRevLett.62.1079
20. K.S. Babu, R.N. Mohapatra, A solution to the strong CP problem without an axion. Phys. Rev. D **41**, 1286 (1990). https://doi.org/10.1103/PhysRevD.41.1286
21. S.M. Barr, D. Chang, G. Senjanovic, Strong CP problem and parity. Phys. Rev. Lett. **67**, 2765–2768 (1991). https://doi.org/10.1103/PhysRevLett.67.2765
22. G. Barenboim, J. Bernabeu, Spontaneous breakdown of CP in left-right symmetric models. Z. Phys. C **73**, 321–331 (1997). https://doi.org/10.1007/s002880050321. arXiv:hep-ph/9603379
23. R. Kuchimanchi, P/CP conserving CP/P violation solves strong CP problem. Phys. Rev. D **82**, 116008 (2010). https://doi.org/10.1103/PhysRevD.82.116008. arXiv:1009.5961 [hep-ph]
24. N.G. Deshpande, J.F. Gunion, B. Kayser, F.I. Olness, Left-right symmetric electroweak models with triplet Higgs. Phys. Rev. D **44**, 837–858 (1991). https://doi.org/10.1103/PhysRevD.44.837
25. A. Patra, S.K. Rai, Lepton-specific universal seesaw model with left-right symmetry. Phys. Rev. D **98**(1), 015033 (2018). https://doi.org/10.1103/PhysRevD.98.015033. arXiv:1711.00627 [hep-ph]
26. K.S. Babu, A. Patra, Higgs boson spectra in supersymmetric left-right models. Phys. Rev. D **93**(5), 055030 (2016). https://doi.org/10.1103/PhysRevD.93.055030. arXiv:1412.8714 [hep-ph]
27. P.-H. Gu, Spontaneous mirror left-right symmetry breaking for leptogenesis parametrized by Majorana neutrino mass matrix. JHEP **10**, 016 (2017). https://doi.org/10.1007/JHEP10(2017)016. arXiv:1706.07706 [hep-ph]
28. M. Mitra, R. Ruiz, D.J. Scott, M. Spannowsky, Neutrino jets from high-mass W_R gauge bosons in TeV-scale left-right symmetric models. Phys. Rev. D **94**(9), 095016 (2016). https://doi.org/10.1103/PhysRevD.94.095016. arXiv:1607.03504 [hep-ph]
29. A. Das, P. Konar, A. Thalapillil, Jet substructure shedding light on heavy Majorana neutrinos at the LHC. JHEP **02**, 083 (2018). https://doi.org/10.1007/JHEP02(2018)083. arXiv:1709.09712 [hep-ph]
30. M.T. Arun, T. Mandal, S. Mitra, A. Mukherjee, L. Priya, A. Sampath, Testing left-right symmetry with an inverse seesaw mechanism at the LHC. Phys. Rev. D **105**(11), 115007 (2022). https://doi.org/10.1103/PhysRevD.105.115007. arXiv:2109.09585 [hep-ph]
31. CMS Collaboration, CMS, the Compact Muon Solenoid: technical proposal. https://cds.cern.ch/record/290969
32. ATLAS Collaboration, ATLAS: technical proposal for a general-purpose pp experiment at the Large Hadron Collider at CERN. https://cds.cern.ch/record/290968
33. C. Brust, P. Maksimovic, A. Sady, P. Saraswat, M.T. Walters, Y. Xin, Identifying boosted new physics with non-isolated leptons. JHEP **04**, 079 (2015). https://doi.org/10.1007/JHEP04(2015)079. arXiv:1410.0362 [hep-ph]
34. Y.B. Zeldovich, I.Y. Kobzarev, L.B. Okun, Cosmological Consequences of the Spontaneous Breakdown of Discrete Symmetry. Zh. Eksp. Teor. Fiz. **67**, 3–11 (1974). https://cds.cern.ch/record/411756
35. T.W.B. Kibble, Topology of cosmic domains and strings. J. Phys. A **9**, 1387–1398 (1976). https://doi.org/10.1088/0305-4470/9/8/029
36. G. Chauhan, P.S.B. Dev, R.N. Mohapatra, Y. Zhang, Perturbativity constraints on $u(1)_{B-L}$ and left-right models and implications for heavy gauge boson searches. J. High Energy Phys. **2019**(1), (2019). https://doi.org/10.1007/jhep01(2019)208
37. B.W. Lee, C. Quigg, H.B. Thacker, Strength of weak interactions at very high energies and the Higgs boson mass. Phys. Rev. Lett. **38**, 883–885 (1977). https://doi.org/10.1103/PhysRevLett.38.883
38. B.W. Lee, C. Quigg, H.B. Thacker, Weak interactions at very high energies: the role of the Higgs-boson mass. Phys. Rev. D **16**, 1519–1531 (1977). https://doi.org/10.1103/PhysRevD.16.1519

39. M.E. Peskin, T. Takeuchi, Estimation of oblique electroweak corrections. Phys. Rev. D **46**, 381–409 (1992). https://doi.org/10.1103/PhysRevD.46.381
40. J. Erler, M. Schott, Electroweak precision tests of the standard model after the discovery of the higgs boson. Prog. Part. Nucl. Phys. **106**, 68–119 (2019). https://doi.org/10.1016/j.ppnp.2019.02.007
41. CMS Collaboration, A. Tumasyan et al., Search for a right-handed W boson and a heavy neutrino in proton–proton collisions at $\sqrt{s}$ = 13 TeV. JHEP **04**, 047 (2022). https://doi.org/10.1007/JHEP04(2022)047. arXiv:2112.03949 [hep-ex]
42. ATLAS Collaboration, G. Aad et al., Search for new resonances in mass distributions of jet pairs using 139 fb^{-1} of pp collisions at $\sqrt{s}$ = 13 TeV with the ATLAS detector. JHEP **03**, 145 (2020). https://doi.org/10.1007/JHEP03(2020)145. arXiv:1910.08447 [hep-ex]
43. ATLAS Collaboration, M. Aaboud et al., Search for a right-handed gauge boson decaying into a high-momentum heavy neutrino and a charged lepton in pp collisions with the ATLAS detector at $\sqrt{s}$ = 13 TeV. Phys. Lett. B **798**, 134942 (2019). https://doi.org/10.1016/j.physletb.2019.134942. arXiv:1904.12679 [hep-ex]
44. CMS Collaboration, A.M. Sirunyan et al., Search for heavy Majorana neutrinos in same-sign dilepton channels in proton–proton collisions at $\sqrt{s}$ = 13 TeV. JHEP. **01**, 122 (2019). https://doi.org/10.1007/JHEP01(2019)122. arXiv:1806.10905 [hep-ex]
45. CMS Collaboration, J.S. Kim, Search for heavy majorana neutrinos in events with same-sign lepton pairs and jets using the CMS detector in pp collisions at $\sqrt{s}$ = 13 TeV. PoS **ICHEP2018**, 892 (2019). https://doi.org/10.22323/1.340.0892
46. O. Mattelaer, M. Mitra, R. Ruiz, Automated neutrino jet and top jet predictions at next-to-leading-order with parton shower matching in effective left-right symmetric models. arXiv:1610.08985 [hep-ph]
47. CMS Collaboration, Searches for dijet resonances in pp collisions at $\sqrt{s}$ = 13 TeV using the 2016 and 2017 datasets. https://cds.cern.ch/record/2637847
48. ATLAS Collaboration, M. Aaboud et al., Search for heavy Majorana or Dirac neutrinos and right-handed W gauge bosons in final states with two charged leptons and two jets at $\sqrt{s}$ = 13 TeV with the ATLAS detector. JHEP **01**, 016 (2019). https://doi.org/10.1007/JHEP01(2019)016. arXiv:1809.11105 [hep-ex]
49. CMS Collaboration, A.M. Sirunyan et al., Search for a heavy right-handed W boson and a heavy neutrino in events with two same-flavor leptons and two jets at $\sqrt{s}$ = 13 TeV. JHEP **05**, 148 (2018). https://doi.org/10.1007/JHEP05(2018)148. arXiv:1803.11116 [hep-ex]
50. S. Aoki, Y. Aoki, D. Becirevic, T. Blum, G. Colangelo, S. Collins, M. Della Morte, P. Dimopoulos, S. Dürr, H. Fukaya, M. Golterman, S. Gottlieb, R. Gupta, S. Hashimoto, U.M. Heller, G. Herdoiza, R. Horsley, A. Jüttner, T. Kaneko, C.-J.D. Lin, E. Lunghi, R. Mawhinney, A. Nicholson, T. Onogi, C. Pena, A. Portelli, A. Ramos, S.R. Sharpe, J.N. Simone, S. Simula, R. Sommer, R. Van de Water, A. Vladikas, U. Wenger, H. Wittig, Flag review 2019, Eur. Phys. J. C **80**(2), (2020). https://doi.org/10.1140/epjc/s10052-019-7354-7
51. HPQCD Collaboration Collaboration, R.J. Dowdall, C.T.H. Davies, R.R. Horgan, G.P. Lepage, C.J. Monahan, J. Shigemitsu, M. Wingate, Neutral b-meson mixing from full lattice qcd at the physical point. Phys. Rev. D **100**, 094508 (2019). https://doi.org/10.1103/PhysRevD.100.094508
52. Y. Zhang, H. An, X. Ji, R.N. Mohapatra, General cp violation in minimal left-right symmetric model and constraints on the right-handed scale. Nucl. Phys. B **802**(1–2), 247–279 (2008). https://doi.org/10.1016/j.nuclphysb.2008.05.019
53. CMS Collaboration, A.M. Sirunyan et al., Combined measurements of Higgs boson couplings in proton–proton collisions at $\sqrt{s}$ = 13 TeV. Eur. Phys. J. C **79**(5), 421 (2019). https://doi.org/10.1140/epjc/s10052-019-6909-y. arXiv:1809.10733 [hep-ex]
54. ATLAS Collaboration, G. Aad et al., Combined measurements of Higgs boson production and decay using up to 80 fb^{-1} of proton–proton collision data at $\sqrt{s}$ = 13 TeV collected with the ATLAS experiment. Phys. Rev. D **101**(1), 012002 (2020). https://doi.org/10.1103/PhysRevD.101.012002. arXiv:1909.02845 [hep-ex]
55. CMS Collaboration, A. Tumasyan et al., Search for a heavy Higgs boson decaying into two lighter Higgs bosons in the $\tau\tau bb$ *final state at 13 TeV*. JHEP **11**, 057 (2021). https://doi.org/10.1007/JHEP11(2021)057. arXiv:2106.10361 [hep-ex]
56. ATLAS Collaboration, G. Aad et al., A search for heavy Higgs bosons decaying into vector bosons in same-sign two-lepton final states in pp collisions at $\sqrt{s}$ = 13 TeV with the ATLAS detector. JHEP **07**, 200 (2023). https://doi.org/10.1007/JHEP07(2023)200. arXiv:2211.02617 [hep-ex]
57. ATLAS Collaboration, G. Aad et al., Search for $t\bar{t}H/A \rightarrow t\bar{t}t\bar{t}$ production in the multilepton final state in proton–proton collisions at $\sqrt{s}$ = 13 TeV with the ATLAS detector. JHEP **07**, 203 (2023). https://doi.org/10.1007/JHEP07(2023)203. arXiv:2211.01136 [hep-ex]
58. ATLAS Collaboration, G. Aad et al., Search for charged Higgs bosons decaying into a top quark and a bottom quark at $\sqrt{s}$ = 13 TeV with the ATLAS detector. JHEP **06**, 145 (2021). https://doi.org/10.1007/JHEP06(2021)145. arXiv:2102.10076 [hep-ex]
59. CMS Collaboration, A. Tumasyan et al., Search for a charged Higgs boson decaying into a heavy neutral Higgs boson and a W boson in proton–proton collisions at $\sqrt{s}$ = 13 TeV. JHEP **09**, 032 (2023). https://doi.org/10.1007/JHEP09(2023)032. arXiv:2207.01046 [hep-ex]
60. Particle Data Group Collaboration, P.A. Zyla et al., Review of Particle Physics. *PTEP* **2020**(8), 083C01 (2020). https://doi.org/10.1093/ptep/ptaa104
61. J. Alwall, R. Frederix, S. Frixione, V. Hirschi, F. Maltoni, O. Mattelaer, H.S. Shao, T. Stelzer, P. Torrielli, M. Zaro, The automated computation of tree-level and next-to-leading order differential cross sections, and their matching to parton shower simulations. JHEP **07**, 079 (2014). https://doi.org/10.1007/JHEP07(2014)079. arXiv:1405.0301 [hep-ph]
62. NNPDF Collaboration, R.D. Ball et al., Parton distributions for the LHC Run II. JHEP **04**, 040 (2015). https://doi.org/10.1007/JHEP04(2015)040. arXiv:1410.8849 [hep-ph]
63. T. Sjöstrand, S. Ask, J.R. Christiansen, R. Corke, N. Desai, P. Ilten, S. Mrenna, S. Prestel, C.O. Rasmussen, P.Z. Skands, An introduction to PYTHIA 8.2. Comput. Phys. Commun. **191**, 159–177 (2015). https://doi.org/10.1016/j.cpc.2015.01.024. arXiv:1410.3012 [hep-ph]
64. DELPHES 3 Collaboration, J. de Favereau, C. Delaere, P. Demin, A. Giammanco, V. Lemaître, A. Mertens, M. Selvaggi, DELPHES 3, A modular framework for fast simulation of a generic collider experiment. JHEP **02**, 057 (2014). https://doi.org/10.1007/JHEP02(2014)057. arXiv:1307.6346 [hep-ex]
65. M. Cacciari, G.P. Salam, G. Soyez, FastJet user manual. Eur. Phys. J. C **72**, 1896 (2012). https://doi.org/10.1140/epjc/s10052-012-1896-2. arXiv:1111.6097 [hep-ph]
66. M. Cacciari, G.P. Salam, Dispelling the N^3 myth for the k_t jet-finder. Phys. Lett. B **641**, 57–61 (2006). https://doi.org/10.1016/j.physletb.2006.08.037. arXiv:hep-ph/0512210
67. G.P. Salam, Towards Jetography. Eur. Phys. J. C **67**, 637–686 (2010). https://doi.org/10.1140/epjc/s10052-010-1314-6. arXiv:0906.1833 [hep-ph]
68. M. Dasgupta, A. Fregoso, S. Marzani, G.P. Salam, Towards an understanding of jet substructure. JHEP **09**, 029 (2013). https://doi.org/10.1007/JHEP09(2013)029. arXiv:1307.0007 [hep-ph]

69. A.J. Larkoski, S. Marzani, G. Soyez, J. Thaler, Soft drop. JHEP **05**, 146 (2014). https://doi.org/10.1007/JHEP05(2014)146. arXiv:1402.2657 [hep-ph]
70. S. Catani, Y.L. Dokshitzer, M.H. Seymour, B.R. Webber, Longitudinally invariant K_t clustering algorithms for hadron hadron collisions. Nucl. Phys. B **406**, 187–224 (1993). https://doi.org/10.1016/0550-3213(93)90166-M
71. S. Catani, Y.L. Dokshitzer, M. Olsson, G. Turnock, B.R. Webber, New clustering algorithm for multi-jet cross-sections in e+ e- annihilation. Phys. Lett. B **269**, 432–438 (1991). https://doi.org/10.1016/0370-2693(91)90196-W
72. J. Thaler, K. Van Tilburg, Identifying boosted objects with N-subjettiness. JHEP **03**, 015 (2011). https://doi.org/10.1007/JHEP03(2011)015. arXiv:1011.2268 [hep-ph]
73. S. Catani, S. Devoto, M. Grazzini, S. Kallweit, J. Mazzitelli, Top-quark pair production at the LHC: fully differential QCD predictions at NNLO. JHEP **07**, 100 (2019). https://doi.org/10.1007/JHEP07(2019)100. arXiv:1906.06535 [hep-ph]
74. G. Cowan, K. Cranmer, E. Gross, O. Vitells, Asymptotic formulae for likelihood-based tests of new physics. Eur. Phys. J. C **71**, 1554 (2011). https://doi.org/10.1140/epjc/s10052-011-1554-0. arXiv:1007.1727 [physics.data-an]. [Erratum: Eur. Phys. J. C 73, 2501 (2013)]
75. FCC Collaboration, A. Abada et al., FCC-hh: the hadron collider: future circular collider conceptual design report volume 3. Eur. Phys. J. ST **228**(4), 755–1107 (2019). https://doi.org/10.1140/epjst/e2019-900087-0
76. M. Nemevšek, F. Nesti, Left-right symmetry at an FCC-hh. Phys. Rev. D **108**(1), 015030 (2023). https://doi.org/10.1103/PhysRevD.108.015030. arXiv:2306.12104 [hep-ph]